

AD 742232

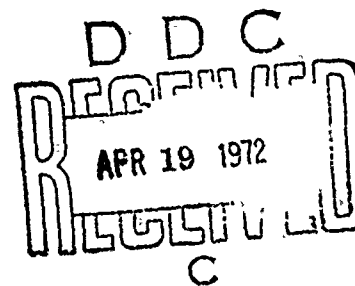
AFATL-TR-71-67

**AERODYNAMIC CHARACTERISTICS
OF
BASIC NOSE-CYLINDER BODIES
FOR
LARGE RANGES OF ANGLE OF ATTACK**

WEAPONS EFFECTS DIVISION

TECHNICAL REPORT AFATL-TR-71-67

JUNE 1971



Approved for public release; distribution unlimited.

Reproduced by
NATIONAL TECHNICAL
INFORMATION SERVICE
Springfield, Va. 22151

AIR FORCE ARMAMENT LABORATORY

AIR FORCE SYSTEMS COMMAND • UNITED STATES AIR FORCE

EGLIN AIR FORCE BASE, FLORIDA

UNCLASSIFIED

Security Classification

DOCUMENT CONTROL DATA - R & D

(Security classification of title, body of abstract and indexing annotation must be entered when the overall report is classified)

1. ORIGINATING ACTIVITY (Corporate author) Weapons Effects Division Air Force Armament Laboratory Eglin Air Force Base, Florida 32542		2a. REPORT SECURITY CLASSIFICATION UNCLASSIFIED	
		2b. GROUP	
3. REPORT TITLE AERODYNAMIC CHARACTERISTICS OF BASIC NOSE-CYLINDER BODIES FOR LARGE RANGES OF ANGLE OF ATTACK			
4. DESCRIPTIVE NOTES (Type of report and inclusive dates) Final Report - October 1969 to June 1971			
5. AUTHOR(S) (First name, middle initial, last name) Robert E. Kellock, Captain, USAF Percy H. MITler, PhD			
6. REPORT DATE June 1971		7a. TOTAL NO. OF PAGES 59	7b. NO. OF REFS 17
8a. CONTRACT OR GRANT NO. F08635-70-C-0053		9a. ORIGINATOR'S REPORT NUMBER(S) AFATL-TR-71-67	
b. PROJECT NO.		9b. OTHER REPORT NO(S) (Any other numbers that may be assigned this report)	
c.			
d.			
10. DISTRIBUTION STATEMENT Approved for public release; distribution unlimited.			
11. SUPPLEMENTARY NOTES Available in DDC		12. SPONSORING MILITARY ACTIVITY Air Force Armament Laboratory Air Force Systems Command Eglin Air Force Base, Florida 32542	
13. ABSTRACT The existing methods of predicting aerodynamic characteristics for basic blunt-based bodies of revolution are reviewed and assessed. Utilizing the more accurate methods, a digital computer program was developed which uses numerical techniques, thus avoiding less accurate simplifying assumptions. This new approach provides reasonable accuracy in predicting the normal force and moment coefficients of basic model combinations for angles of attack ranging from zero to 90 degrees. This accuracy in prognosis also includes freestream Mach numbers ranging from subsonic to hypersonic.			

UNCLASSIFIED

Security Classification

14.	KEY WORDS	LINK A		LINK B		LINK C	
		ROLE	WT	ROLE	WT	ROLE	WT
	Blunt-based bodies of revolution Aerodynamic characteristics Normal force and moment coefficients Digital computer program						

UNCLASSIFIED

Security Classification

**Aerodynamic Characteristics
of
Basic Nose-Cylinder Bodies
for
Large Ranges of Angle of Attack**

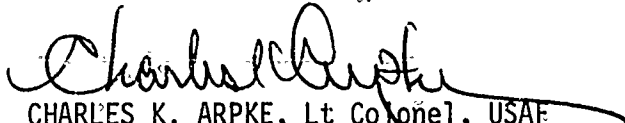
**Robert E. Kellock, Captain, USAF
Percy H. Miller, Ph.D.**

Approved for public release; distribution unlimited.

FOREWORD

This report is based on a master's degree thesis presented by the author to the graduate faculty of the Louisiana State University in 1971. The Air Force Armament Laboratory recommended that it be prepared and published as a technical report since all research was performed by an Air Force student at the cited educational institution. The research was accomplished during the October 1969 - June 1971 period and was identified and encouraged through contracts F08635-68-C-0107 and F08635-70-C-0053; also, related project number 2543, "Aerodynamics of Bodies at High Angle of Attack". Acknowledgement for assistance and guidance is extended to Mrs. V. B. Harvey and Mr. W. E. Stant (DLOS).

This technical report has been reviewed and is approved.


CHARLES K. ARPKE, Lt Colonel, USAF
Chief, Weapons Effects Division

ABSTRACT

The existing methods of predicting aerodynamic characteristics for basic blunt-based bodies of revolution are reviewed and assessed. Utilizing the more accurate methods, a digital computer program was developed which uses numerical techniques, thus avoiding less accurate simplifying assumptions. This new approach provides reasonable accuracy in predicting the normal force and moment coefficients of basic model combinations for angles of attack ranging from zero to 90 degrees. This accuracy in prognosis also includes freestream Mach numbers ranging from subsonic to hypersonic.

Approved for public release; distribution unlimited.

TABLE OF CONTENTS

Section		Page
I	INTRODUCTION	1
II	REVIEW OF THEORIES	2
	1. Munk's Potential Theory	2
	2. Allen's Work	2
	3. Kelly's Interpretation	3
	4. Supersonic Potential Flow	7
	5. Boundary Layer Corrections	7
	6. Previous Results	7
III	DISCUSSION	8
	1. Transient Effect	8
	2. Cross-Flow Drag Coefficient	11
	3. End Effects	11
	4. Nose Radius	14
	5. Half-Angle	14
	6. DCMDA and DCNDA	16
IV	PROGRAM DESCRIPTION	17
	1. Program Information	17
	2. Main Program	17
	3. Subsonic Subroutine	17
	4. Supersonic Subroutines	17
	5. Second Term Integral	21
	6. Cross-Flow Drag Coefficient	21
	7. Transient Effects	21
	8. Radius	21
	9. Theta	26
	10. Drag Correction for Finite Length	27
	11. DCNDA	27
	12. DCMDA	27
	13. Output	29
V	RESULTS	32
	1. Subsonic	32
	2. Supersonic	35
	3. Indicated Improvements	35
VI	FUTURE DEVELOPMENT	42
REFERENCES		43
APPENDIX		45

LIST OF FIGURES

Number	Title	Page
1	Schwabe's Transient Drag Coefficient	5
2	Model at Angle of Attack Schematic	6
3	Plot of k_1 and k_2 (Munk)	6
4	Limit of Schwabe's Results	9
5	Approximation of Transient Effect	10
6	Crossflow Drag Coefficient	12
7	Goldstein's Correction for Finite Length	12
8	Gowen and Perkins' Experimental Results	13
9	Nose Radius Computation Methods	15
10	Initial Normal Force Slope	16
11	Comparisons to Experimental Data - Subsonic	33
12	Comparisons to Experimental Data - Supersonic	36

LIST OF TABLES

Number	Title	Page
I	Program Information	18
II	Main Program	19
III	Subsonic Subroutine	20
IV	Supersonic Subroutine	22
V	Second Term Integral of Normal Force and Moment	23
VI	Drag Coefficient for Cylinder at Crossflow Mach and Reynolds Numbers	24
VII	Cylinder Cross-Flow Drag Coefficient Transient Factor	25
VIII	Radius at Any Given X	26

LIST OF TABLES (Concluded)

Number	Title	Page
IX	Theta for the Nose Model Being Considered	26
X	Drag Coefficient Correction for Finite Length	27
XI	DCNDA	28
XII	DCMDA	28
XIII	Output (Left Half)	30
XIV	Output (Right Half)	31

LIST OF SYMBOLS

A	= Apparent mass factor - transverse = $1 + k_1$
A_p	= Planform area
A_R	= Reference area for coefficients (base area)
B	= Apparent mass factor - longitudinal = $1 + k_2$
C_D	= Drag coefficient (D/qA)
C_{d_c}	= Crossflow drag coefficient
C_L	= Lift coefficient (L/qA)
C_m	= Moment coefficient (M/qAd)
C_N	= Normal force coefficient (N/qA)
d	= Model diameter, one caliber
EL	= Length measured from nearest end of the model
F	= Force
k_1	= Apparent mass factor transverse - Munk
k_2	= Apparent mass factor longitudinal - Munk
ℓ	= Model length
M	= Moment (about model base)
M_c	= Crossflow Mach number
N	= Normal flow
q	= Freestream dynamic pressure
q_c	= Crossflow dynamic pressure
r	= Radius of model
S_B	= Area of base

t = time
 U = Freestream velocity
 V = Model volume
 V_c = Crossflow velocity
 x = Axial position on model
 x_c = Axial position of centroid of planform area
 x_m = Axial position of moment reference (base)
 α = Angle of attack
 η = Drag correction factor for finite length
 η_i = Local drag correction factor for finite length
 θ = Model surface angle = $\arctan dr/dx$
 θ_v = Nose half-angle
 ρ = Density

SECTION I

INTRODUCTION

The efficient design of missiles requires accurate predictions of aerodynamic characteristics. The early missile designers were forced to test models of their design in wind tunnels to obtain these predictions. But as the flow about bodies became better described by theory, methods of calculating the aerodynamic characteristics were devised. However, these methods are valid only for a rather narrow range of flow conditions. As the theories were advanced and improved, the predictions became more accurate, and the limitations with regard to such parameters as angle of attack and Mach number became less restrictive. This is not to mean that the Mach number and angle-of-attack ranges were large.

Recently, changing requirements for the purpose and general structure of missiles require predicting the aerodynamic characteristics for smaller length-to-diameter ratios over larger ranges of angle of attack and Mach number. This study provides advances to existing computational techniques and furnishes greater flexibility with regard to these parameters. The results are limited to basic nose-cylinder combinations featuring pointed noses and blunt bases because no evaluations of blunt nose - cylinder combinations were included.

To accomplish the objective of the study, a computerized document search provided about 17,000 report abstracts, and about 1,400 were selected for more careful examination. Of these, some 400 were obtained for further study. A review of these reports showed that very little experimental data was available in the region of interest; therefore, the effort for the study was shifted from an empirical study to a review and more thorough examination of theories. An analysis of the more successful methods indicated that a digital computer program might be produced to easily apply these methods to simple model combinations. By avoiding the limiting assumptions that were commonly imposed, it appeared that the accuracy could be extended to the region of interest.

This study, then, represents the first stage of an effort to produce a method that will accurately predict aerodynamic characteristics for complex missile configurations.

SECTION II

REVIEW OF THEORIES

1. MUNK'S POTENTIAL THEORY

Most of the successful theories related to this study have begun with the classical work of Munk presented in Reference 1 and expanded by Kelly in Reference 2 and 3. Munk used potential flow theory to show that the force distribution on an airship is given by:

$$dF = \frac{\rho U^2}{2} (k_2 - k_1) \frac{dS}{dx} \sin 2\alpha \, dx \quad (1)$$

In this expression, S is the surface area, α is the angle of attack, x is the distance along the longitudinal axis, and $(k_2 - k_1)$ is the apparent mass factor for the difference in longitudinal and transverse flow. Equation (1) integrates to zero for an airship, but if the body has a flat base of area S_B , the result is a finite force:

$$\text{Lift} = \int dF = \frac{\rho U^2}{2} (k_2 - k_1) S_B \sin 2\alpha \quad (2)$$

Since Munk's research was concerned with very small angles of yaw, this potential force is referenced to the wind vector as lift. At higher angles of attack, this estimate would yield increasing error because the forces due to viscous effects had not been included.

2. ALLEN'S WORK

Allen, in Reference 4, assumes that the viscous forces are independent of the potential flow, and the lift and moment coefficients are written as the sum of two terms; namely, the potential term and a viscous term.

$$C_L = (k_2 - k_1) \frac{S_B}{A_R} \sin 2\alpha \cos \frac{\alpha}{2} + n C_{dC} \frac{A_D}{A_R} \sin^2 \alpha \cos \alpha \quad (3a)$$

$$C_m = \left[\frac{V - S_B (\ell - x_m)}{A_R} \right] (k_2 - k_1) \sin 2\alpha \cos \frac{\alpha}{2} + n C_{dC} \frac{A_D}{A_R} (x_m - x) \sin^2 \alpha \quad (3b)$$

The first term is Munk's potential theory as modified by Ward in Reference 5 to show that the potential cross force is directed midway between the normals to the longitudinal axis and the wind vector. The A_R represents the reference area for the coefficients, V is the volume of the model, and ℓ is the total length. In the second (viscous) term, C_{d_c} refers to the cylinder steady-state two-dimensional drag coefficient for two-dimensional flow. The value of η corrects this drag coefficient for finite model length according to values tabulated by Goldstein in Reference 6. The x_m is the moment reference point, x_c is the centroid of the planform area, A_p , and $\sin^2 \alpha$ comes from the resolution of dynamic pressure from the P crossflow velocity $U \sin \alpha$ to the free-stream velocity.

3. KELLY'S INTERPRETATION

Kelly, in References 2 and 3, deals with the normal force coefficient which eliminates the factor $\cos \alpha$ in the second term of Equation (3a). This method also eliminates the need to assume that the axial drag component of the lift force is negligible.

Allen, in Reference 4, presents the viscous contribution to the cross force from a cylindrical element of length dx as:

$$dF = 2r C_{d_c} (\rho V_c^2 / 2) dx \quad (4)$$

where r is the body radius at point x ($r = r(x)$), and V_c is the cross-flow velocity. Kelly resolved the free-stream dynamic pressure, q , into cross-flow and axial components and corrected the cross-flow drag coefficient for finite length with η . Defining the normal force and moment coefficient as:

$$C_N = N/qA \quad (5a)$$

$$C_m = M/qAd \quad (5b)$$

(where d is the body diameter), the coefficient increments due to viscous cross-flow are:

$$\Delta C_N = \frac{2\eta \sin^2 \alpha}{A_R} \int_0^\ell r C_{d_c} dx \quad (6a)$$

$$\Delta C_m = \frac{2\eta \sin^2 \alpha}{A_R} \int_0^l r C_{d_c} (x_m - x) dx \quad (6b)$$

These terms are entirely due to viscous effects, since C_{d_c} will not exist for a true potential flow.

Allen was aware that the viscous term drag coefficient C_{d_c} should be related to the transient effect as presented by Schwabe in Reference 7. Schwabe found that the drag coefficient for a circular cylinder in cross-flow starting from rest varies according to the parameter $V_c t/r$, where t is elapsed time (Figure 1). The steady-state value of C_{d_c} for Schwabe's experiment was approximately one. Kelly considered a lamina of air, dx thick, moving along the body axis at speed $U \cos \alpha$ and across the body at speed $U \sin \alpha$. He postulated that the cross-flow senses an impulsive flow about a circular cylinder of radius r (Figure 2); hence, the Schwabe time parameter is redefined as

$$\frac{V_c}{r} t = \frac{U \sin \alpha}{r} \frac{x}{U \cos \alpha} = \frac{x \tan \alpha}{r} \quad (7)$$

To aid integration, Kelly approximated Schwabe's curve (Figure 1) with a portion of an arc tangent function, $y = \tan^{-1} x$, and then approximated the arc tangent function with a truncated Taylor series. This permitted rapid evaluation of the function without reference to a table of values.

Allen had used a laminar value of 1.2 for C_{d_c} , based on the cross-flow Reynolds number. In Reference 8, Hill C_{d_c} notes that Kelly used a turbulent value of 0.35 when the free-stream Reynolds number indicated the boundary layer to be turbulent. The observation made was that if the axial boundary layer is turbulent, the cross-flow layer will behave in a turbulent manner, even though the cross-flow Reynolds number is well below that associated with transitions (References 3, 8).

To evaluate the factor $(k_2 - k_1)$, Kelly replaced it with $(AB/2) \cos^2 \theta$, where $A = 1 + k_1$, $B = 1 + k_2$, and $\tan \theta = dr/dx$ (Figure 3). This approach has been compared to the work presented by Upson and Klikoff in Reference 9.

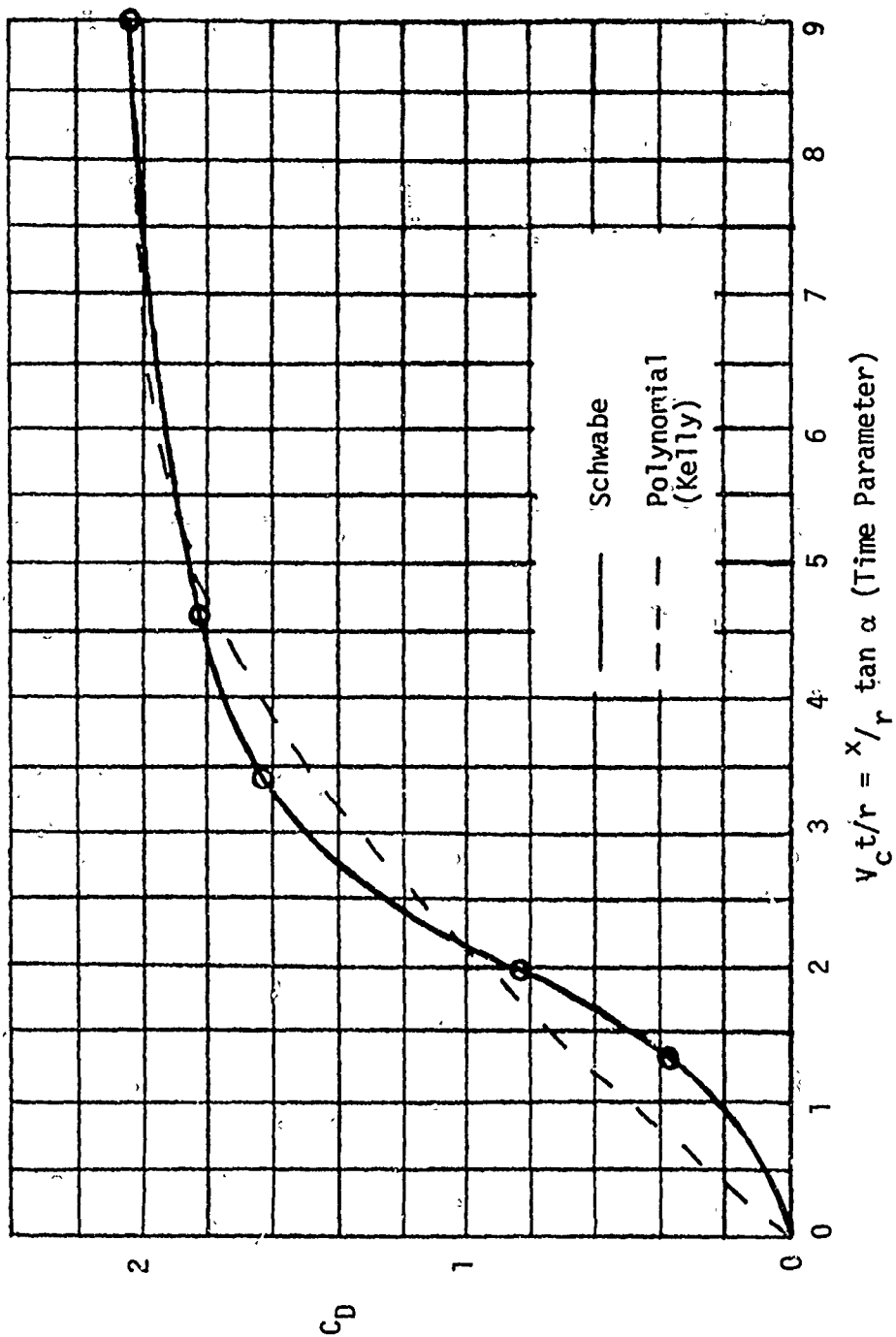
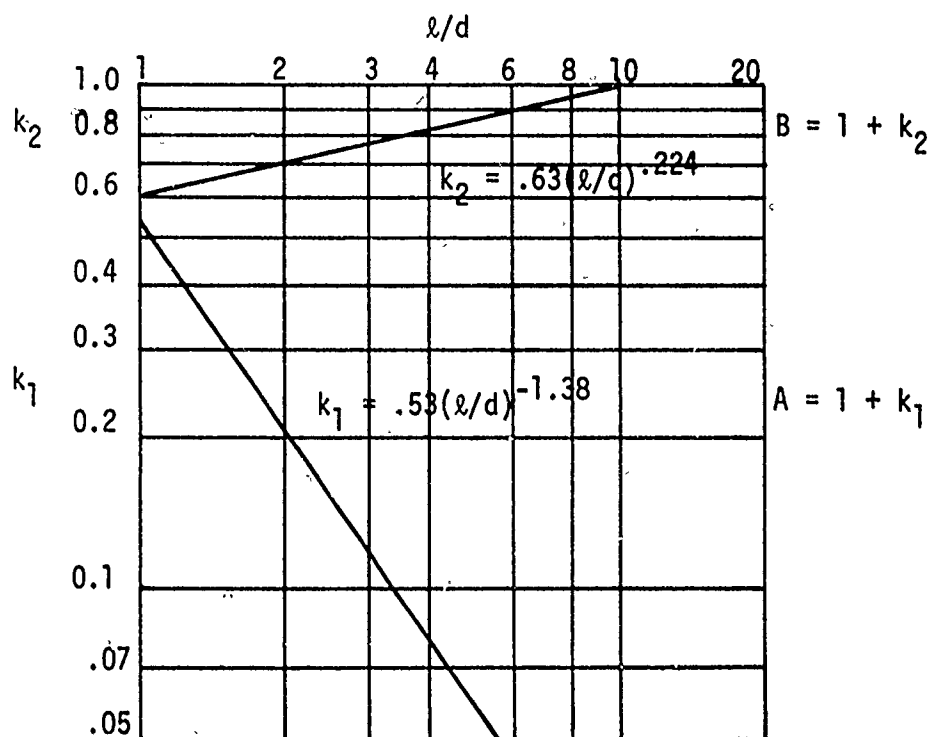
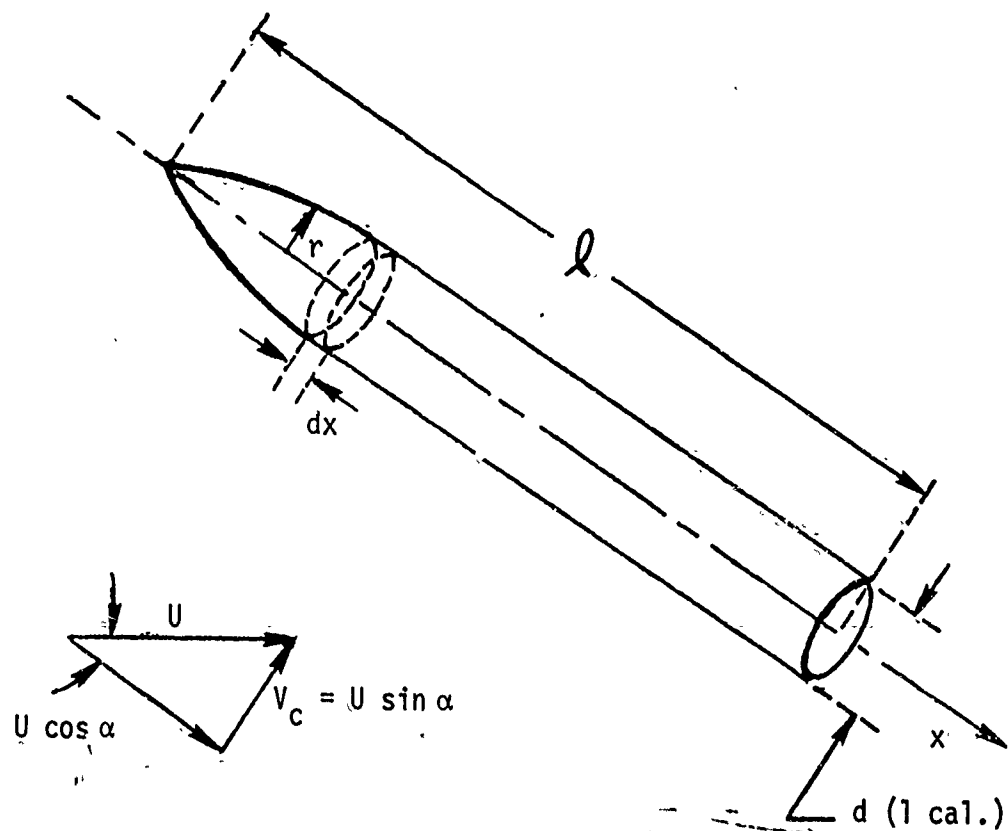


Figure 1. Schwabe's Transient Drag Coefficient



4. SUPERSONIC POTENTIAL FLOW

Except for vehicles with slender noses, Munk's theory is not accurate for supersonic flow; hence, Kelly used the second order theory presented by Van Dyke in Reference 10 for this flow region. This changes the potential terms of the coefficient expressions to

$$\Delta C_N = \left(\frac{dC_N}{d\alpha} \right)_{\alpha=0} \sin \alpha \cos \alpha \quad (8a)$$

$$\Delta C_m = \left(\frac{dC_m}{d\alpha} \right)_{\alpha=0} \sin \alpha \cos \alpha \quad (8b)$$

5. BOUNDARY LAYER CORRECTIONS

Kelly, in his calculations, also included model size increases due to thickening of the boundary layer as the flow progressed along the body length. These relatively small corrections (about 5% for a 14 caliber missile at $\alpha = 8$ degrees, and $M = 2.87$, and about 4% for a 9 caliber model at $\alpha = 30$ degrees and $M = 0.26$) are most applicable to slender bodies at small angles of attack. As the angle of attack becomes larger, the distance a particle flows along the body becomes smaller until at $\alpha = 90$ degrees there is no flow along the body, but only cross-flow. These corrections are generally small and not significant at relatively large angles of attack for the models used in this study; therefore, they will not be considered in this report.

6. PREVIOUS RESULTS

Kelly was able to achieve excellent results up to about 30 degrees angle of attack for subsonic flow, and up to 10 degrees for supersonic flow. With minor computational changes, he also has produced reasonably good predictions up to 40 or 45 degrees for both cases.

SECTION III

DISCUSSION

The success achieved by Kelly shows that the basic approach is sound, and further extension is possible. A simple modular digital computer program allows for more precise evaluation of the various parameters. More specifically, such a program permits the rapid calculation of the aerodynamic characteristics even though the parameters may vary over the large ranges.

1. TRANSIENT EFFECT

The transient evaluated by Schwabe's experiments limited Kelly's method to a time parameter value of nine ($x/r \tan \alpha \approx 9$), since Schwabe's experiments did not define the transient effect beyond this value. This limit is expressed as angle of attack versus model length in Figure 4. Schwabe's limiting factor was the size of his equipment. He showed a maximum C_d of 2.07 at the maximum time parameter. The data points show a leveling off of the drag coefficient, but no indication of how it returns to a steady-state value.

The first computations of the computer program indicated a slight over-prediction of normal force coefficient near the parameter value of nine for subsonic cases. The supersonic cases showed an extensive over-prediction at nearly all time parameter values in the transient region.

The drag buildup for a cylinder normal to impulsive flow is attributed to the formation of vortices. As movement begins, an upstream displacement of the fluid occurs over a broad front. The flow field quickly forms, and begins to narrow as vortices are developed. As velocity increases, the vortices begin to be shed, and the wake narrows to near steady-state conditions. The narrowing of the wake results in a cross-flow drag reduction.

Schwabe's experiments were conducted in a water tank of a length that prevented his experiment from reaching steady-state conditions. It is a reasonable assumption that the upstream effect was influenced by the confines of the tank length and resulted in an erroneous drag increase and delayed the onset of the reduction towards steady-state flow. Based on a knowledge of these limitations, a reduction of the transient maximum to 1.97 at a time parameter of seven is used. A linear decline to the steady-state drag coefficient at a time parameter of ten is used to provide continuity of the function (Figure 5). Since upstream effects provide a major part of the transient phenomena, the supersonic case does not utilize any transient effect.

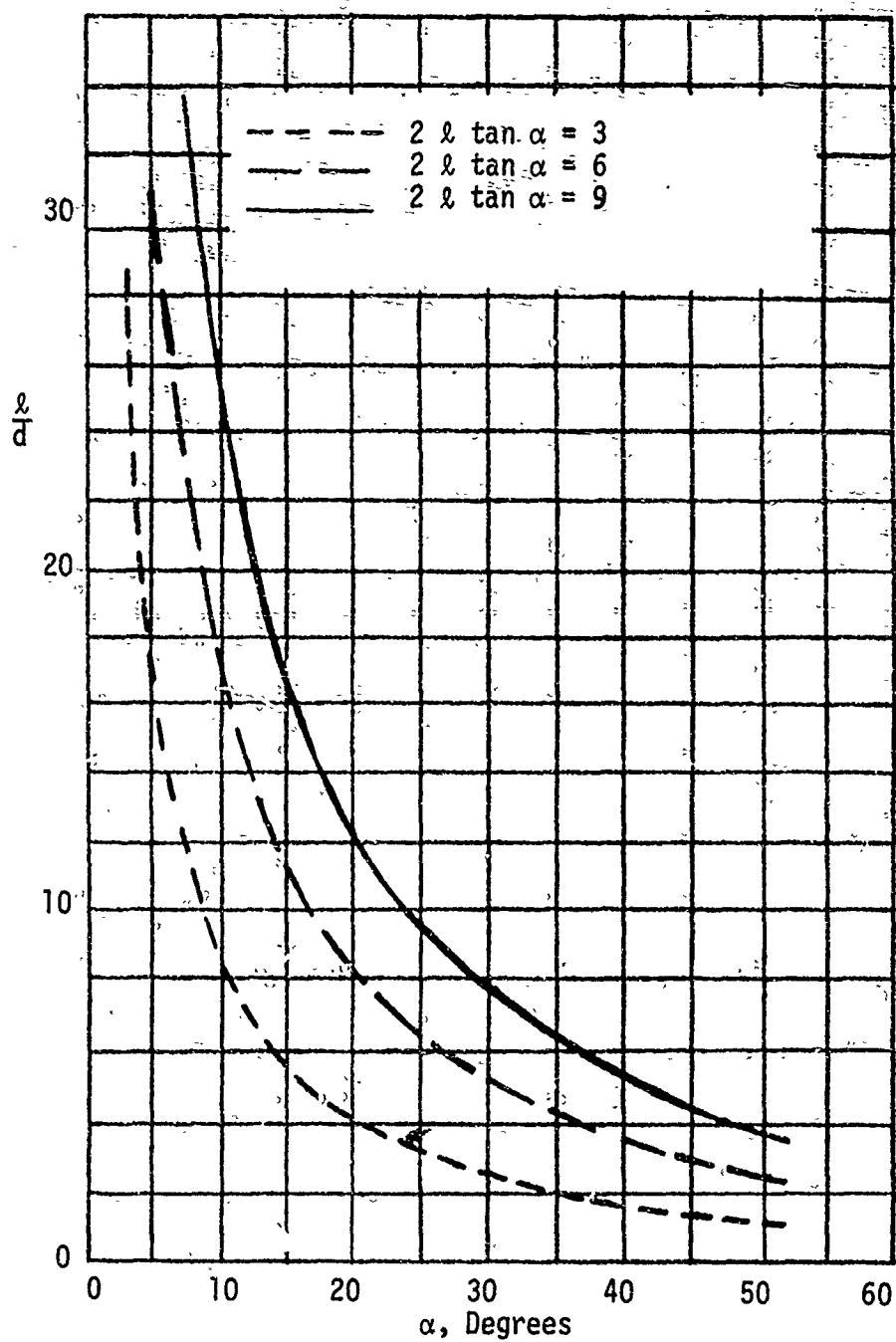


Figure 4. Limit of Schwabe's Results

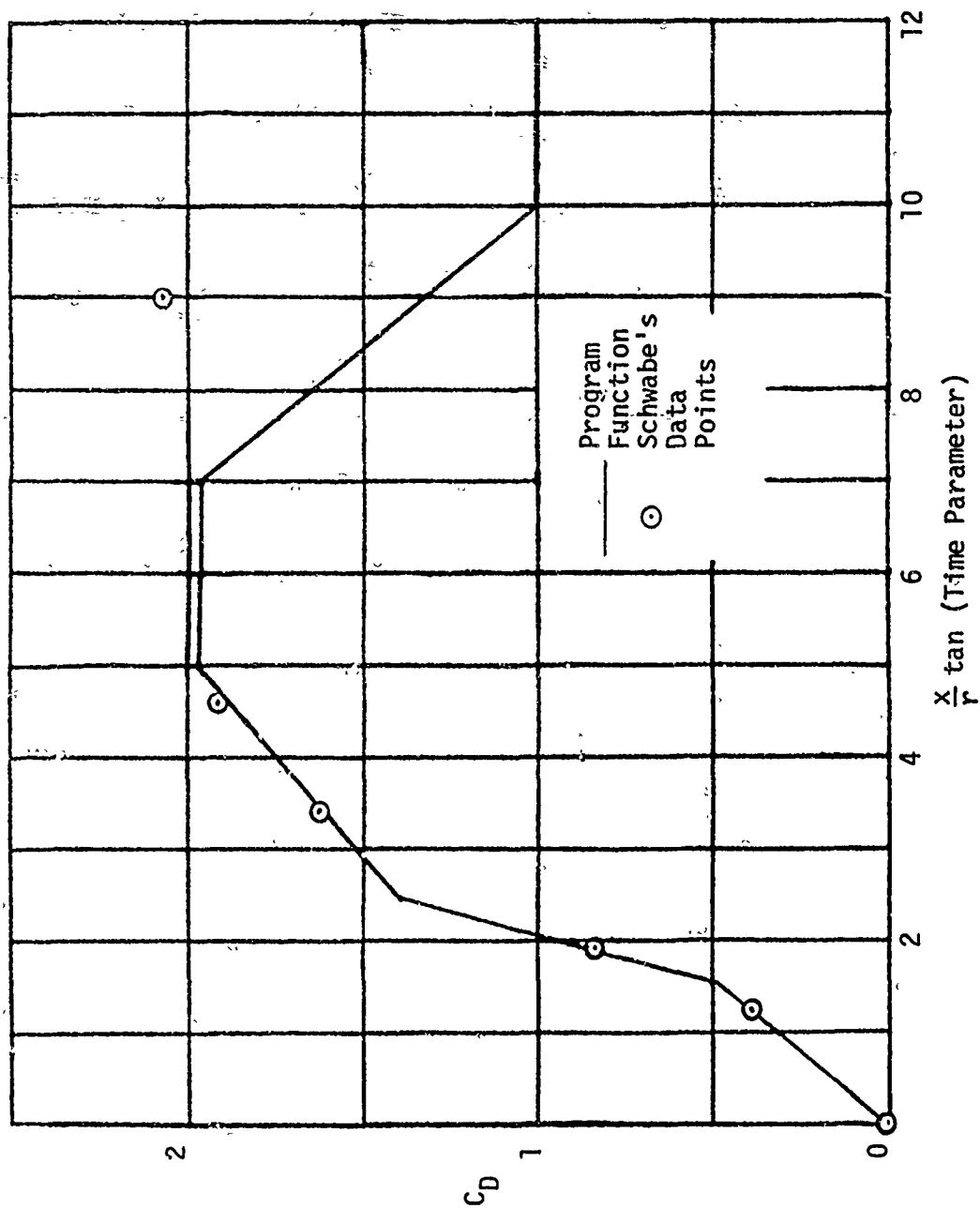


Figure 5. Approximation of Transient Effect

Schwabe's experiments were conducted at a Reynolds number of 580, for which the steady-state drag coefficient (Reference 11) is about 1.15. Schwabe's curve is therefore normalized by this value and is used as a transient factor to apply to the actual two-dimensional drag coefficient for the model and flow conditions being considered.

2. CROSS-FLOW DRAG COEFFICIENT

The cross-flow drag coefficient is a function of the cross-flow Mach number and Reynolds number. To develop this function, two-dimensional data from several sources are combined. In Reference 11, Hoerner shows an assortment of data at various Mach and Reynolds numbers. His plots of C_d versus Mach number agree with most other reports, but they are not continuous where the magnitude of the Reynolds number causes the transition from laminar to turbulent flow to occur below a Mach number of approximately 0.55. Transition causes a flat-bottomed dip in the drag coefficient (Reference 12) for Reynolds numbers between approximately 300,000 and 700,000. Above Mach 0.55, compressibility effects appear to dominate the flow and suppress any Reynolds number effects.

To compute this dip in the cross-flow drag coefficient curve, a Reynolds number is computed. The characteristic length used in this computation is that which the freestream senses, and it is expressed as $l = 2r \sin \alpha + x \cos \alpha$. Freestream velocity is used in the computation, based on evidence that the cross-flow boundary layer appears to assume the character of the axial boundary layer.

The drag curves obtained from Reference 11 are approximated by straight line segments for the computer function. Another straight line segment provides transition from the laminar curve to the turbulent curve as the Reynolds number increases from 400,000 to 500,000 (Figure 6).

3. END EFFECTS

The two-dimensional drag coefficient must be corrected for finite cylinder length. Goldstein's data tabulated in Reference 6 gives an overall, or average, ratio of C_d to $C_{d_{inf}}$ (Figure 7).

Since a portion of the computer program developed for this study uses a strip technique (numerical integration by trapezoid rule), the local correction referenced to the nearest end, rather than the average value, must be used. The drag coefficient distribution is not clearly indicated in any of the references examined except in Gowen and Perkin's report (Reference 12). Efforts to curve-fit these data (Figure 8) led to the choice of the following algebraic function to express η_i :

$$\eta_i = 1 - \exp[-(M_c + 1)\sqrt{EL}] \quad (9)$$

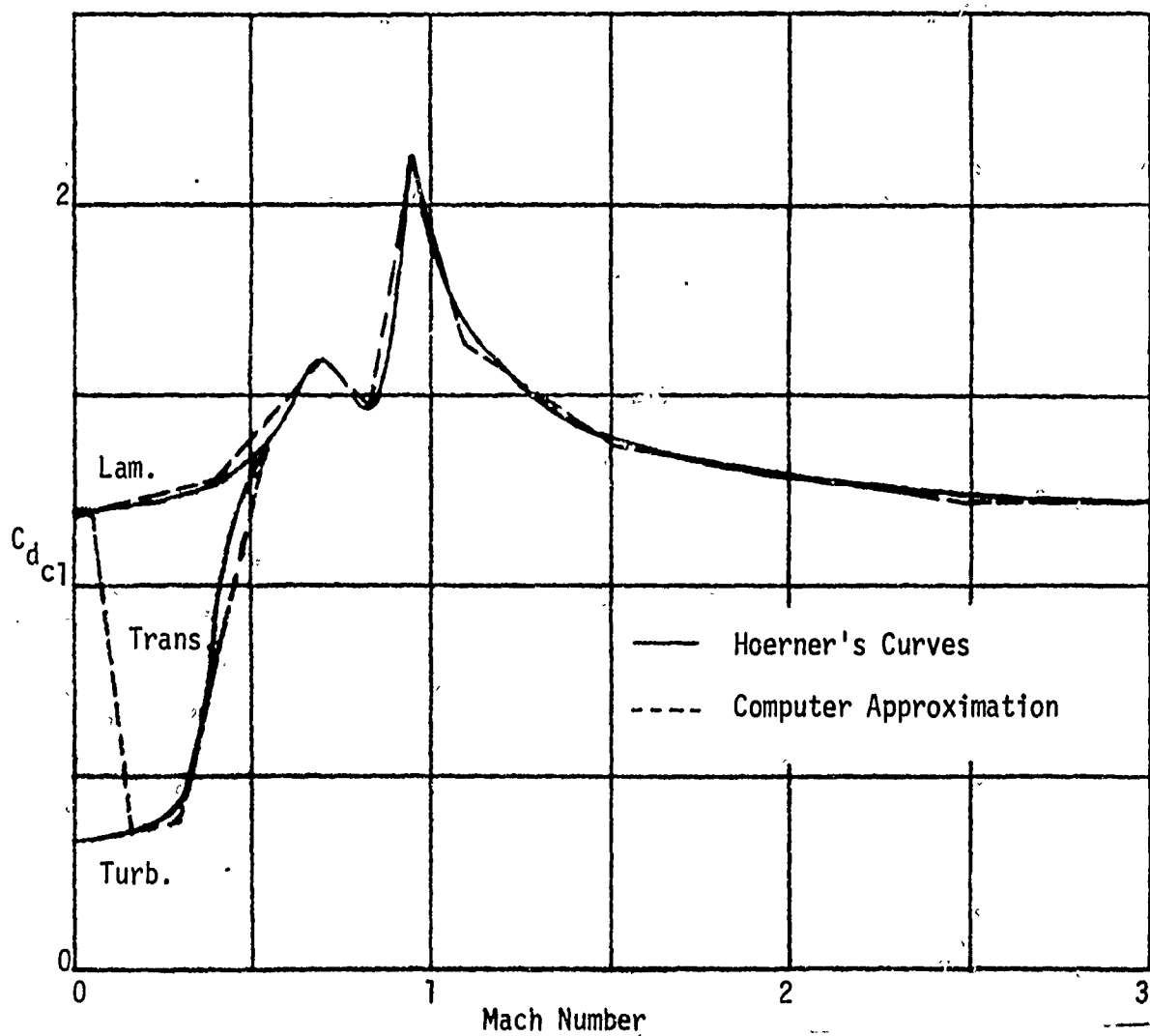


Figure 6. Crossflow Drag Coefficient

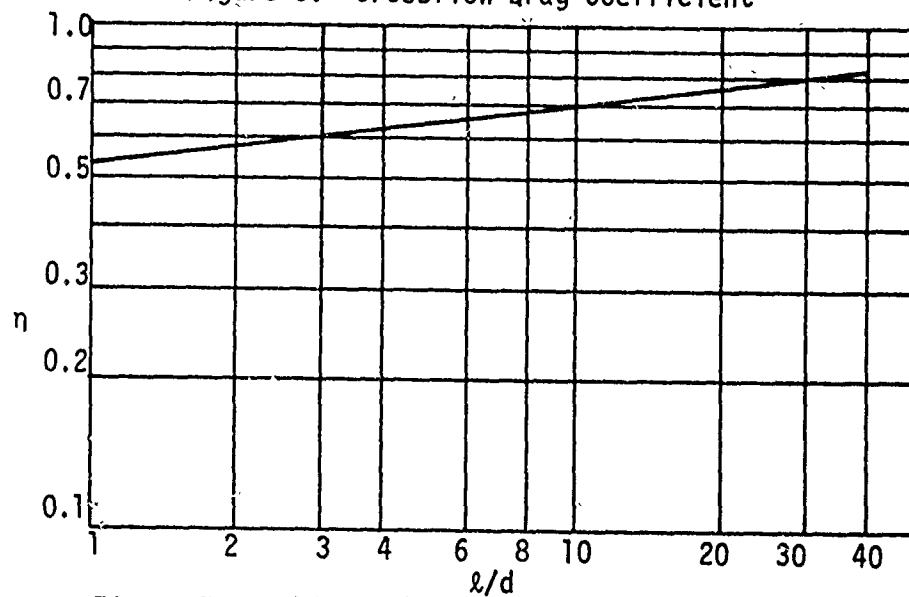


Figure 7. Goldstein's Correction for Finite Length

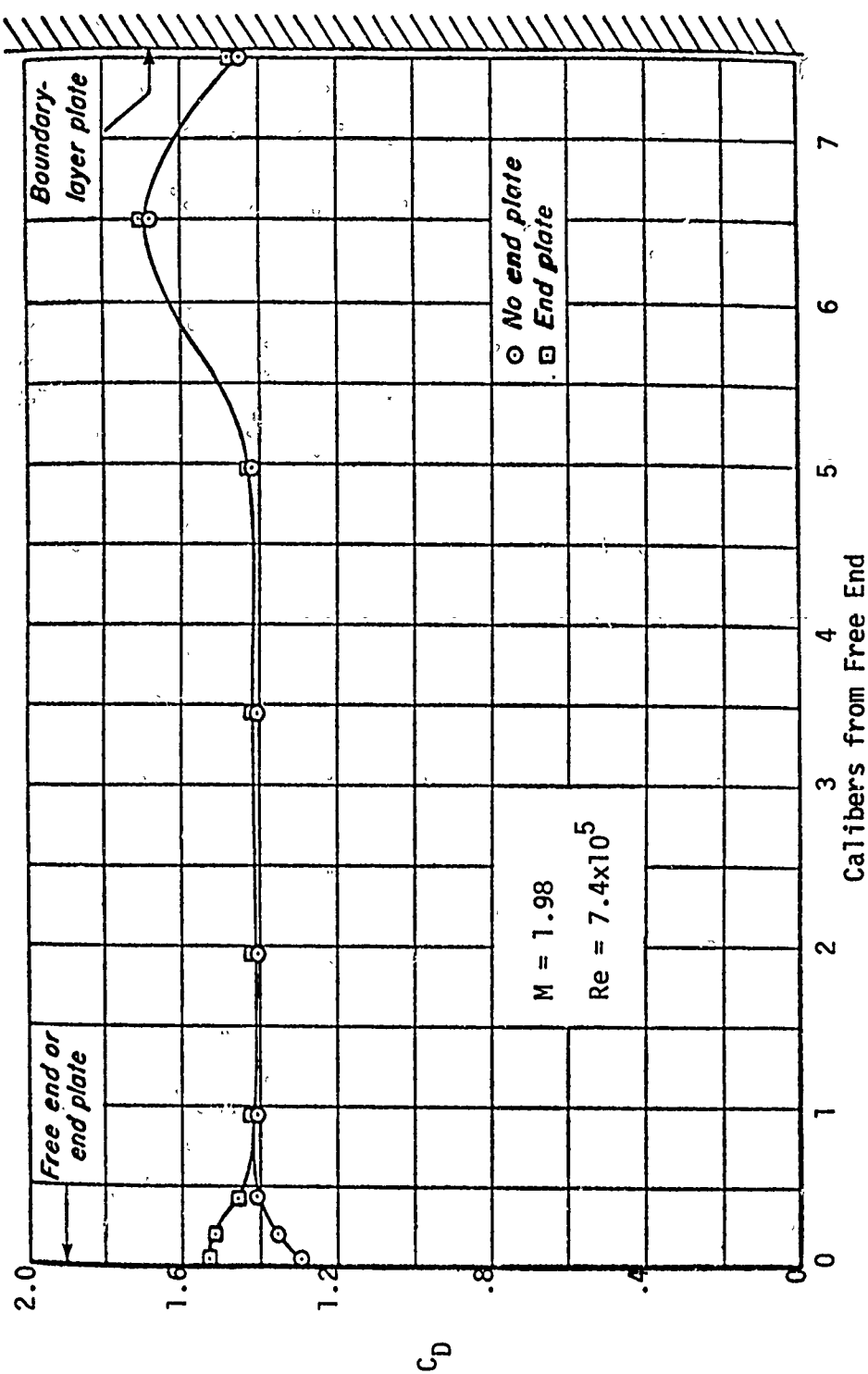


Figure 8. Gowen and Perkins' Experimental Results (from Reference 12)

EL is the distance from the nearest end of the model, and the quantity $(M_\infty + 1)$ arises from the fact that the end effects diminish rapidly with increasing Mach number. This is confirmed by Penland in Reference 13, where end effects have been determined to be virtually non-existent for Mach 6.86.

Since these end effect corrections apply to right circular cylinders, further corrections are required for a vehicle with a pointed nose. As the nose becomes more slender, the end effects increase and the local drag coefficient returns to that for a right cylinder. Thus, the drag reduction due to end effects is further reduced by the oblique flow around a pointed nose. If the nose half-angle is near zero degrees, the flow is essentially the same as a cylinder of equal length. If the nose half-angle is near 90 degrees, the end effect is so drastically reduced that almost no drag is contributed by the nose portion of the model. These observations indicate that the end effect change due to nose half-angle follows the form of the cosine of the nose half-angle. Therefore, when the strip being computed lies on the nose portion of the model, the η_i computed is reduced by multiplication with the cosine of the nose half-angle.

4. NOSE RADIUS

Computation of the transient effect, the nose half-angle, and the two-dimensional drag coefficient requires that the radius at any axial point be available. Since the commonly used nose shapes include cones, tangent ogives, secant ogives, power series, and parabolics, a variable function is used to express radius variation with axial distance. Based on a nose-type code, the applicable function is selected for each computation (Figure 9).

A tangent ogive function is used for both ogives, since including a function for a secant ogive would be more complex than necessary at this stage. Power series and parabolic nose shapes are approximated by power series expression, and cones are defined by a tangent function. None of the functions employed account for any nose blunting; hence, this analysis is valid only for pointed noses. However, minor blunting would introduce only minor error in the results.

5. HALF-ANGLE

The computation of the apparent mass factor $AB/2 \cos^2 \theta_v$ requires an average value of θ_v ($= \tan^{-1} dr/dx$) over the entire model. Also, the computation of η_i requires the use of the nose half-angle. (For power series and parabolic noses, the local half-angle would increase accuracy but this additional complication is not included at this stage.) To compute these factors, the average nose half-angle is computed by ten increments of $\Delta r/\Delta x$, each equal to one-tenth of the nose length. In the computations, this value is proportioned, or weighted, according to nose length divided by the total model length in order to obtain an average value of θ for the model.

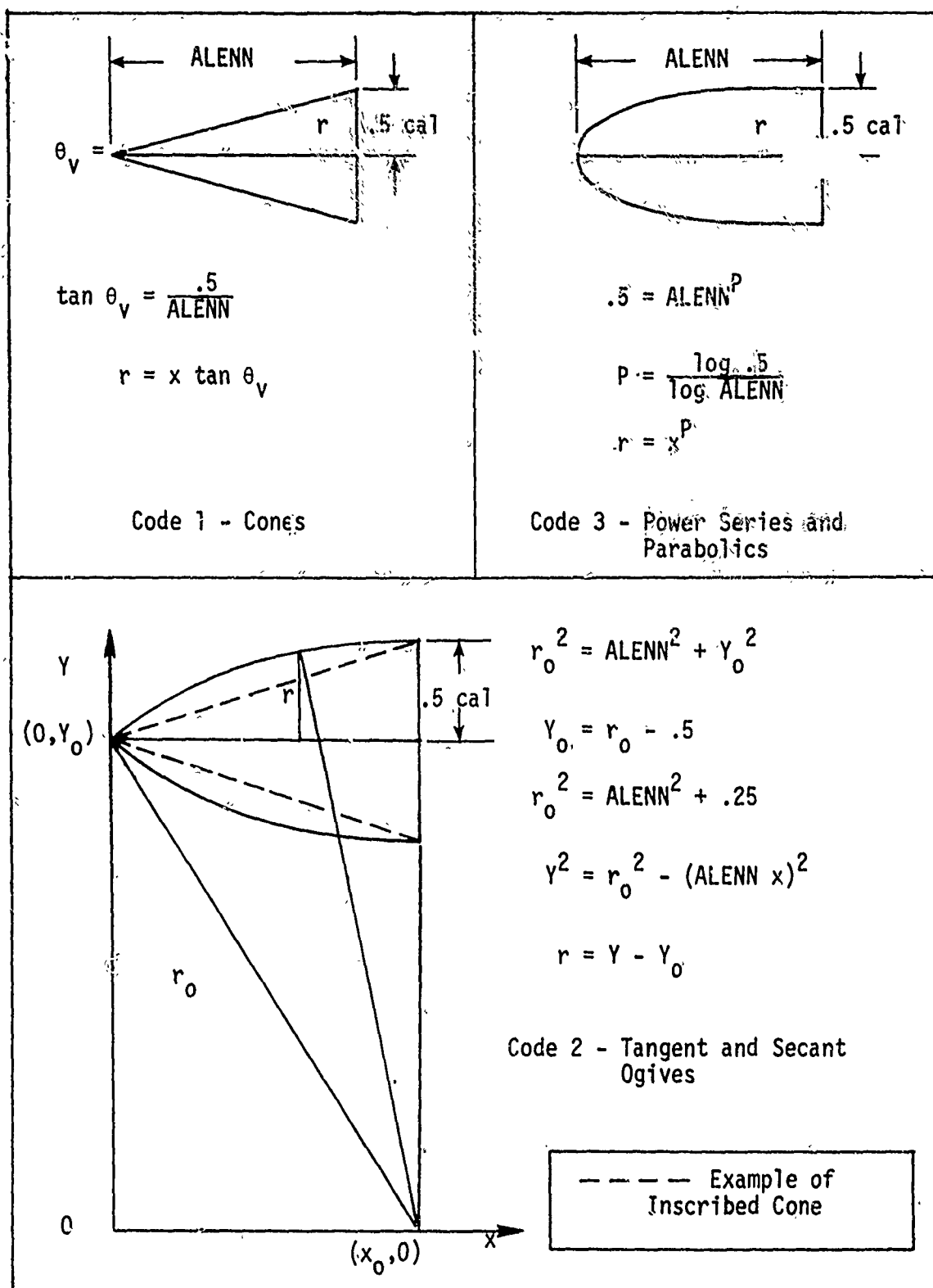


Figure 9. Nose Radius Computation Methods

6. DCMDA AND DANDA

The supersonic potential flow term requires the determination of values for the derivatives $(dC_m/d\alpha)_\alpha = 0$ and $(dC_N/d\alpha)_\alpha = 0$ for the particular model being considered. If these values are available from experimental data or other sources, they may be read into the computer program on the input data cards. If they are not read in as data, two functions will be used to approximate them.

The approximation of Grimminger, Williams, and Young (Reference 14) for ogives and cones and afterbodies, (Figure 10) is used as a starting point for these functions. (For purposes of these functions, power series and parabolic noses have been grouped together with ogives.) These curves are further approximated by straight line segments, with corrections for Mach number. Through logic switching, the result produced is an approximate function subroutine. The application is limited to cone half-length (inscribed cone for noses not true cones) from five to fifteen degrees. Comparisons with other data (Reference 2) indicate reasonable agreement. Since potential force is a minor part of the total normal force in the region of interest, the approximation is adequate.

The $dC_m/d\alpha$ is computed by multiplying the $dC_N/d\alpha$ by the moment arm, measured from the model center of pressure to the model base. Accuracy of the results has suffered somewhat since no particular effort has been made to accurately predict the moment of the center of pressure for varying model dimensions or flight conditions. The inclusion of these factors would significantly complicate the method of this study. When additional experimental data are available, further study of these refinements would be in order.

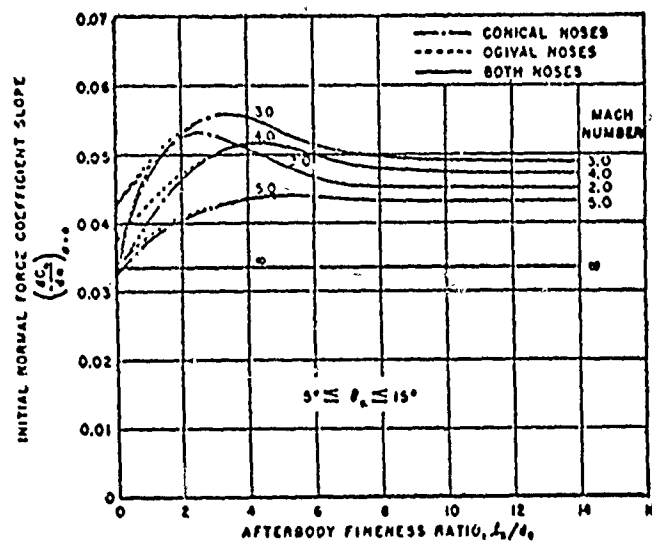


Figure 10. Initial Normal Force Slope (From Reference 14)

SECTION IV

PROGRAM DESCRIPTION

The computer program resulting from this study is written for the IBM 360 Model 65 as installed in the Louisiana State University Computer Research Center. The WATFIV compiler, which gives complete syntax and logic analysis with explicit error descriptions, was used to insure an accurate and rapid transition from one phase of the program development to the next. Some of the special capabilities of this load-and-go compiler were utilized; consequently, changes in the program might be required if another type of computer was used.

1. PROGRAM INFORMATION

The computer program information is provided by a series of comment cards which define the variables, codes, and terms used in the program (Table I).

2. MAIN PROGRAM

The main program controls the overall operation of the computer program (Table II). This program provides a means of data input, terminates execution, writes output headings (which include input data), and exercises logic to differentiate between subsonic and supersonic computation techniques.

The input data for each case are read from a single card. They include a nose-type code, the nose length and model length (both in calibers), the freestream Mach number, the Reynolds number per caliber divided by the Mach number, and the constants $(dC_N/d\alpha) = 0$ and $(dC_M/d\alpha) = 0$ if experimental or other source data are to be used. The program termination is based on a nose-type code of zero, which is supplied by a blank card at the end of the data stack. The next statements call the proper subroutine for the case being considered, and then returns to the input step for either the next case or termination.

3. SUBSONIC SUBROUTINE

The subroutine that directs the computation for the subsonic case is shown in Table III. It computes constants, initializes incremental variables, increments the angle of attack, computes the first (potential) term, calls another subroutine for the second (viscous) term, and prints out the computed values. All dimensional constants are computed in calibers. Some constants are computed through the use of additional subprograms, which will be described.

TABLE I. PROGRAM INFORMATION

```

*****
N - NOSE TYPE      0= CALL EXIT, 1= CONE, 2= OGIVE, PARABOLIC, 3= POWER
AMN - REYNOLDS NUMBER PER CALIBER DIVIDED BY MACH NUMBER
P - POWER FACTOR OF POWER SERIES NOSE
X- LONGITUDINAL AXIS, AFT OF NOSE IS POSITIVE      XN,XO- NEW, OLD X
ALENN,ALENN,ALENA - LENGTH OF NOSE, MODEL, AND AFTERBODY IN CALIBERS
AM- MACH NO.      SB- AREA OF BASE      SP- AREA OF PLANFORM
AMC - CROSSEFLOW MACH NUMBER FOR CROSSEFLOW DRAG COEFFICIENT
RN, RO - NEW, OLD RADIUS      D - REFERENCE DIAMETER, BASE DIAMETER
A - ANGLE OF ATTACK, FROM FREESTREAM TO LONGITUDINAL AXIS
V - VOLUME OF MODEL      THET - INCREMENT OF THETA, DELTA R/DELTA THETA
THEN, THEN - EQUIVALENT HALF ANGLE OF NOSE, MODEL
ETA - DRAG CORRECTION FACTOR FOR CROSSEFLOW ON A FINITE CYLINDER
EL - LENGTH IN CALIBERS FROM THE END OF THE MODEL FOR ETA COMP.
FSTTMM- FIRST TERM OF NORMAL FORCE      R - RADIUS OF MODEL AT X
FSTTMM - FIRST TERM OF MOMENT ABOUT BASE      TP- TIME PARAMETER FOR CDC
SECTN,SECTM- SECOND TERM NORMAL, MOMENT INCREMENT
SECTIN,SECTIM - SECOND TERM NORMAL, MOMENT INTEGRAL
CSUGN - NORMAL FORCE COEFFICIENT      CSUBM - MOMENT COEFFICIENT
DCNDA, DCMDA - NORMAL FORCE, MOMENT COEFFICIENT SLOPE VERSUS ALPHA
AKIL- APPARENT MASS FACTOR, LONGITUDINAL      MUNK-WARD
BK2T- APPARENT MASS FACTOR, TRANSVERSE      MUNK-WARD
AMF - APPARENT MASS FACTOR      AB OVER 2 TIMES COSINE SQUARED THETA
CSDC - CYLINDER CROSSEFLOW DRAG COEFFICIENT FOR SPECIFIED R AND X
CD - CYLINDER DRAG COEFFICIENT FOR CROSSEFLOW MACH AND REYNOLDS NUMBERS
ARM - ESTIMATED MOMENT ARM TO COMPUTE DCMDA FROM DCNDA
*****

```

TABLE II. MAIN PROGRAM

```

*****
1 READ (5,10) N,ALENN, ALENM, AM, AMN, DCNDA, DCMDA
10 FORMAT (I5,3F10.5,F10.0,2F10.5)
   IF (N.EQ.0) GO TO 3
   WRITE (6,11) N, ALENN, ALENM, AM, AMN
11 FORMAT (I11,///10X,
1      'RUN OF NOSE CODE',I2,' MODEL, WITH A',F 6.2,' CALIBE
   ER NOSE,',F5.2,' AND AN OVERALL LENGTH OF',F 6.2,' CALIBERS. MACH N
   UMBER IS',F5.2,'/5X, 'AND RE(PER CAL) OVER MACH NO. IS',F8.0,'/
1//12X,'ALPHA',9X,'CSUBN',8X,'CSUBM',7X,'FSTTMN',7X,'SECTMN',7X,
1'FSTTMM',7X,'SECTMM',9X,'CD',/80('---'))
   IF (AM.LT.1.0) GO TO 2
   CALL SUBSON(N,ALENN,ALENM,AM,AMN,DCNDA,DCMDA)
   GO TO 1
2 CALL SUBSON (N,ALENN,ALENM,AM,AMN)
   GO TO 1
3 STOP      END
*****

```

TABLE III. SUBSONIC SUBROUTINE

```

SUBROUTINE SUBSON (N,ALENN,ALENM,AM,AMN)
SB=J.14159/4. SP=ALENM-ALENN/2. V=(ALENM-2.*ALENN/3.)*SB
DELA=5.*3.14159/180. CSUBN =0. CSUBM =0. A=0.
AK1L=1.+0.53*ALENM**(-1.38)
BK2T=1.+0.63*ALENM**.224
IF (ALENM.GT.10.) BK2T=1.0
CALL THETA (N,ALENN,ALENM,THEN,THEM)
AMF=(AK1L*BK2T/2.)*COS(THEN)**2
WRITE (6,12) A , CSUBN, CSUBM
1 A=A+DELA
FSTTMN=AMF*(SB/SB)*SIN(2.*A)*COS(A/2.)
FSTTMM=AMF*(V/SB)*SIN(2.*A)*COS(A/2.)
CALL SECTI (N,ALENN,ALENM,A,CD,AMN,AM,SECTIN,SECTIM,THEN)
SECTMN=(2.*SIN(A)**2/SB)*SECTIN
SECTMM=(2.*SIN(A)**2/SB)*SECTIM
CSUBN=(FSTTMN+SECTMN)
CSUBM=(FSTTMM+SECTMM)
AD=A*180./3.14159
WRITE (6,13) AD, CSUBN, CSUBM,FSTTMN, SECTMN,FSTTMM, SECTMM, CD
12 FORMAT (10X,3(F 6.2,8X)/)
13 FORMAT (10X,8(F 6.2,8X)/)
2 IF(AD.LT.87.5) GO TO 1
3 RETURN
END

```

4. SUPERSONIC SUBROUTINES

The subroutine that directs the computation for the supersonic case is shown in Table IV. It differs from the subsonic subroutine in the computation of the first (potential) term. It also provides values for $(dC_N/d\alpha) = 0$ and $(dC_M/d\alpha)_\alpha = 0$ when they have not been supplied as data in the main program.

5. SECOND TERM INTEGRAL

The subroutine that computes the integral portion of the second (viscous) terms of the normal force and moment coefficients is shown in Table V. It initializes incremented variables, sets the increment for trapezoid integration for the nose portion, and sets the initial value of x as one-half an increment ahead of the nose. After incrementing x , it computes the radius, selects the drag coefficient, corrects it for transient effect and finite length, then computes the incremental value. When the value of x reaches the last increment on the nose portion, it is increased a half-increment to equal the nose length, the increment size is changed, x is reset one-half increment forward of the beginning of the afterbody, and the integration is continued. For the afterbody portion, the radius remains constant and is defined outside the integration loop.

6. CROSS-FLOW DRAG COEFFICIENT

The function that computes the drag coefficient for the integration subroutine is shown in Table VI. Using the cross-flow Mach number, the function selects one of eight equations. Then, if the cross-flow Mach number is below 0.55, the free-stream Reynolds number is computed. If it is in the transition region, the drag coefficient is adjusted by one of two functions.

7. TRANSIENT EFFECTS

The function that corrects the cross-flow drag coefficient for the transient effect is shown in Table VII. If the cross-flow Mach number is greater than one, no correction is made. Otherwise, the time parameter is calculated, and one of six functions is selected to compute the correction factor.

8. RADIUS

The function that computes the radius at any point on the model nose is shown in Table VIII. The proper nose type is determined from the nose-type code, then the appropriate function is selected. For the power series and parabolic noses, a simple relation is used to generate an exponent, and the radius is computed. The ogives are represented by the function for tangent ogives. Radii for cones are computed from the tangent of the nose half-angle.

TABLE IV. SUPERSONIC SUBROUTINE

```

SUBROUTINE SUPSON (N,ALENN,ALENM,AM,AMN,DCNDA,DCMDA)
SB=3.14159/4. SP=ALENM-ALENN/2. A =0.
DELA=5.*3.14159/180. CSUBN =0. CSUBM =0.
CALL THETA (N,ALENN,ALENM,THEN,THEM)
IF (DCNDA.EQ.0.) DCNDA=CNA(N,ALENN,ALENM,AM)
IF (DCMDA.EQ.0.) DCMDA=CMA(DCNDA,ALENM,AM)
WRITE (6,11) DCNDA, DCMDA
WRITE (6,12) A , CSUBN, CSUBM
1 A=A+DELA
FSTTMN=DCNDA*SIN(A)*COS(A)
FSTTM=DCMDA*SIN(A)*COS(A)
CALL SECTI (N,ALENN,ALENM,A,CD,AMN,AM,SECTIN,SECTIM,THEN)
SECTMN=(2.*SIN(A)**2/SB)*SECTIN
SECTMM=(2.*SIN(A)**2/SB)*SECTIM
CSUBN = FSTTMN+SECTMN
CSUBM = FSTTM+SECTMM
AD=A*180./3.14159
WRITE (6,13) AD, CSUBN, CSUBM,FSTTMN, SECTMN,FSTTM, SECTMM, CD
11 FORMAT (10X,DCNDA IS ',F6.2,', AND DCMDA IS ',F6.2/')
12 FORMAT (10X,3(F 6.2,8X)/)
13 FORMAT (10X,8(F6.2,8X)/)
2 IF(AD.LT.87.5) GO TO 1
3 RETURN
END

```

TABLE V. SECOND TERM INTEGRAL OF NORMAL FORCE AND MOMENT

```

SUBROUTINE SECTI (N,ALENN,ALENNM,A,CD,AMN,AM,SECTIN,SECTIM,THEN)
  SECTIN=0.      DELX=ALENN/10.      SECTIM=0.      X=-DELX/2.
1  X=X+DELX      R=RADIUS(N,X,ALENN)
  CD=CDRM (A,AM,AMN,R,X)      CSDC= CDC (A,R,X,CD,AM)
  ETA=DCORR (X,ALENN,THEN,AM,A,ALENN)      SECTN=R*CSDC*DELX*ETA
  SECTM=R*CSDC*(ALENN-X)*DELX*ETA
  SECTIN=SECTIN+SECTN      SECTIM=SECTIM+SECTM
  IF(X.LT.(ALENN-DELX)) GO TO 1
  X=X+DELX/2
  DELX=(ALENN-ALENN)/10.
  X=X-DELX/2.      R=.5
2  X=X+DELX      CD=CDRM (A,AM,AMN,R,X)
  CSDC= CDC (A,R,X,CD,AM)      ETA=DCORR (X,ALENN,THEN,AM,A,ALENN)
  SECTN=R*CSDC*DELX*ETA      SECTM=R*CSDC*(ALENN-X)*DELX*ETA
  SECTIN=SECTIN+SECTN      SECTIM=SECTIM+SECTM
  IF(X.LT.(ALENN-DELX)) GO TO 2
3  RETURN      END

```

TABLE VI. DRAG COEFFICIENT FOR CYLINDER AT CROSSFLOW MACH AND REYNOLDS NUMBERS

```

FUNCTION CDRM (A,A*,AMN,R,X)
AMC=AM* SIN(A)
REYN= AM*AMN*(2*PI*SIN(A)+X*CC5(A))
IF (RFYN.LI.400000.) GO TO 10
IF (REYN.LI.500000.) GO TO 8
IF (AMC.LI.0.35) GO TO 11
IF (AMC.LI.0.55) GO TO 12
IF (AMC.LI.0.40) GO TO 1
10 IF (AMC.LI.0.70) GO TO 2
13 IF (AMC.LI.0.83) GO TO 3
IF (AMC.LI.0.94) GO TO 4
IF (AMC.LI.1.1) GO TO 5
IF (AMC.LI.1.5) GO TO 6
IF (AMC.LI.2.5) GO TO 7
CDRM=1.22 GO TO 9
1 CDRM= 1.18 + .225*AMC GO TO 9
2 CDRM= 0.93 + 1.1 *AMC GO TO 9
3 CDRM=2.3-AMC GO TO 9
4 CDRM=-3.59+6.1*AMC GOTO 9
5 CDRM=4.95-3.*AMC GO TO 9
6 CDRM=2.45-.726*AMC GO TO 9
7 CDRM=1.57-.14*AMC GO TO 9
11 CDRM= 0.32 + .225*AMC GO TO 9
12 CDRM=-1.375+5.1*AMC GO TO 9
8 CDRM=4.6-0.0000085*REYN
9 RETURN END

```

TABLE VII. CYLINDER CROSS-FLOW DRAG COEFFICIENT TRANSIENT FACTOR

```

FUNCTION CDC (A,R,X,CD,AM)
AMC=AM*5/IN(A)      IF (AMC.GT.1.) GO TO 7
TP=X*IAN(A)/R
IF (TP.LT.1.52) GO TO 1
IF (TP.LT.2.46) GO TO 2
IF (TP.LT.5.00) GO TO 3
IF (TP.LT.7.00) GO TO 4
IF (TP.LT.10.0) GO TO 5
7 CDCF = 1.15/1.15      GO TO 6
1 CDCF = (.316*TP)/1.15      GO TO 6
2 CDCF = (-.59+.968*TP)/1.15      GO TO 6
3 CDCF = (0.83+.229*TP)/1.15      GO TO 6
4 CDCF=1.97/1.15      GO TO 6
5 CDCF = (3.89-.273*TP)/1.15      GO TO 6
6 CDC=CDCF*CD      RETURN      END

```

TABLE VIII. RADIUS AT ANY GIVEN X

```

FUNCTION RADIUS (N,X,ALENN)
  IF (N.EQ.1) GO TO 2
  IF (N.EQ.2) GO TO 1
  P=ALOG(.5)/ALOG(ALENN)
  RADIUS=X**P      GO TO 3
1  UR=ALENN**2+.25
  Y=SQRT(UR**2-(X-ALENN)**2)
  RADIUS=Y-UR+.5   GO TO 3
2  RADIUS=(.5/ALENN)*X
3  RETURN      END

```

9. THETA

The theta subroutine that computes the average change in radius with respect to axial length is shown in Table IX. First, cones are considered, and the nose angle is computed directly. Next, incremented variables are initialized, and the increment is computed. Using the radius function, the radius is computed at each increment and compared to that of the previous increment. These values are summed to obtain an average nose angle. Finally, the nose angle is proportioned to the total model length to get an average angle for the model.

TABLE IX. THETA FOR THE NOSE MODEL BEING CONSIDERED

```

SUBROUTINE THETA (N,ALENN,ALENM,THEN,THEM)
  IF (N.EQ.1) GO TO 2
  THEN =0.      X=0.      DELX=ALENN/10.      RO=0.
1  X=X+DELX
  RN=RADIUS(N,X,ALENN)
  RC=RN-RO
  THET=ATAN(RC/DELX)
  THEN =THEN +.1*THET      RO=RN
  IF (X.LT.(ALENN-DELX/2.)) GO TO 1      GO TO 3
2  THEN =ATAN(.5/ALENN)
3  THEM =THEN *ALENN/ALENM
4  RETURN      END

```

10. DRAG CORRECTION FOR FINITE LENGTH

The function that corrects the two-dimensional drag coefficient for finite length is shown in Table X. The length from the nearest end is computed first, then, the cross-flow Mach number and the square root of the end length are used to compute a correction. If the point being considered is on the nose, another adjustment is made.

TABLE X. DRAG COEFFICIENT CORRECTION FOR FINITE LENGTH

```
FUNCTION DCCORR (X,ALENM,THEN,AM,A,ALENN)
FL=X      IF (X.GT.ALENM/2.) EL= ALENM - X
AMC=AM*SIN(A)   ARGEXP=(AMC+1.)*SQRT(EL)
DCCORR=1.-EXP(-ARGEXP)
IF (X.LT.ALENN) DCCORR = DCCORR*COS(THEN)
RETURN      END
```

11. DCNDA

The DCNDA function that computes the initial slope of the normal force coefficient when plotted against the angle of attack is shown in Table XI. After the afterbody length is determined, a branch to the correct Mach number is taken. For each Mach number branch, a function is selected to correspond to nose type and afterbody length. Finally, the value is converted from ΔC_N per degree to ΔC_N per radian.

12. DCMDA

The DCMDA function that approximates the initial slope of the moment coefficient when plotted against angle of attack is shown in Table XII. It computes the length of the moment arm from a function which describes the movement of the center of pressure versus Mach number. This arm is then applied to the DCNDA supplied from the argument list to obtain DCMDA.

TABLE XI. DCNDA

TO COMPUTE DCNDA, IF NOT SUPPLIED.
 THETA-SUB-V FROM 5 TO 15 DEGREES

```

FUNCTION CNA (N,ALENN,ALENM,AM)
  ALENA=ALENM-ALENN
  IF (AM.LT.2.5) GO TO 10
  IF (AM.LT.3.5) GO TO 6
  IF (AM.LT.4.5) GO TO 2
  IF (ALENA.GT.4.) GO TO 1
  CNA= .032 + .003*ALENA - .02*(AM-5.)      GO TO 14
1  CNA=.043      GO TO 14
2  IF (ALENA.GT.4.5) GO TO 4
  IF (N.GT.1) GO TO 3
  CNA= .033 + .004*ALENA - .04*(AM-4.)      GO TO 14
3  CNA= .038 + .003*ALENA - .05*(AM-4.)      GO TO 14
4  IF (ALENA.GT.8.0) GO TO 5
  CNA= .052 + .001*ALENA - .04*(AM-4.)      GO TO 14
5  CNA=.047      GO TO 14
6  IF (ALENA.GT.3.5) GO TO 8
  IF (N.GT.1) GO TO 7
  CNA= .033 + .006*ALENA - .03*(AM-3.)      GO TO 14
7  CNA= .043 + .004*ALENA - .04*(AM-3.)      GO TO 14
8  IF (ALENA.GT.8.0) GO TO 9
  CNA= .056 + .001*ALENA - .03*(AM-3.)      GO TO 14
9  CNA=.049      GO TO 14
10 IF (ALENA.GT.2.5) GO TO 12
  IF (N.GT.1) GO TO 11
  CNA= .033 + .010*ALENA - .03*(AM-2.)      GO TO 14
11 CNA= .043 + .005*ALENA - .04*(AM-2.)      GO TO 14
12 IF (ALENA.GT.7.0) GO TO 13
  CNA= .053 + .002*ALENA - .08*(AM-2.)      GO TO 14
13 CNA=.045
14 CNA=CNA*1E0./3.14159      RETURN      END

```

TABLE XII. DCMDA

TO COMPUTE DCMDA, IF NOT SUPPLIED

```

FUNCTION CMA (DCNDA,ALENM,AM)
  ARM=(.75-.053*AM)*ALENM
  CMA=DCNDA*ARM      RETURN      END

```

13. OUTPUT

The output format is shown in Tables XIII and XIV. The values printed at zero angle of attack are to remind the reader that the procedures used are all based on simple bodies of revolution which create only drag (no normal force or moment) when the angle of attack is zero. The drag coefficient printed is that of the last increment of integration on the model afterbody, without corrections for transient effect and finite length effect.

TABLE XIII. OUTPUT (LEFT HALF)

RUN OF NOSE CODE 1 MODEL. WITH A 2.83 CALIBER NOSE,
AND AN OVERALL LENGTH OF 8.83 CALIBERS. MACH NUMBER IS 6.84
AND RE (PER CAL) OVER MACH NO. IS 22700.

ALPHA	CSURN	CSUBM	FSTTMN
DCNDA IS	2.46, AND	DCMDA IS	8.43
0.00	0.00	0.00	
5.00	0.24	0.81	0.21
10.00	0.85	3.11	0.42
15.00	1.43	5.22	0.62
20.00	2.14	7.84	0.79
25.00	2.97	10.93	0.94
30.00	3.92	14.44	1.07
35.00	4.92	18.17	1.16
40.00	5.95	22.00	1.21
45.00	6.97	25.82	1.23
50.00	7.95	29.51	1.21
55.00	8.87	32.96	1.16
60.00	9.69	36.07	1.07
65.00	10.39	38.73	0.94
70.00	10.95	40.88	0.79
75.00	11.35	42.44	0.62
80.00	11.58	43.37	0.42
85.00	11.63	43.63	0.21
90.00	11.50	43.23	0.00

TABLE XIV. OUTPUT (RIGHT HALF)

SECTMM	FSTTMM	SECTMM	CD
0.02	0.73	0.08	1.59
0.43	1.44	1.67	1.59
0.81	2.11	3.11	1.32
1.35	2.71	5.13	1.24
2.03	3.23	7.70	1.22
2.85	3.65	10.79	1.22
3.76	3.96	14.21	1.22
4.74	4.15	17.85	1.22
5.74	4.21	21.61	1.22
6.74	4.15	25.36	1.22
7.71	3.96	29.00	1.22
8.62	3.65	32.42	1.22
9.45	3.23	35.50	1.22
10.16	2.71	38.17	1.22
10.73	2.11	40.33	1.22
11.16	1.44	41.92	1.22
11.42	0.73	42.90	1.22
11.50	0.00	43.23	1.22

SECTION V

RESULTS

The computer program was executed more than 40 times, with over 25 runs producing useable data. Many paired runs were made to observe the effect of changing a single parameter or constant. Near the final stages of the program development, a separate regression program was used to fit one set of experimental data. A function of the form $(\text{constant}) \sin \alpha \cos \alpha + (\text{constant}) \sin^3 \alpha / \cos \alpha$ was used for this regression program, since it represents the alpha-dependent quantities of the theory. The high degree of conformity indicated the method was of the proper form.

Three sources were used for comparisons with the output of the program. Almost no data for the desired angle-of-attack range are available. Additional data are required for angle of attack up to 90 degrees, particularly at transonic speeds.

The moment coefficient will not be discussed in detail, since the normal force is calculated for incremental areas, and if it is accurate and no couples exist, the moment must also be accurate. This can be observed from comparisons with the moment data in References 15 and 16, where deviations in normal force coefficient are reflected almost directly in the moment coefficient.

1. SUBSONIC

The subsonic runs were compared with Hauer and Kelly's data in Reference 15 which reports primarily on the Magnus effect of spinning projectile models, but also presents data for a zero spin rate. As shown in Figure 11, the computed values of the coefficients generally take the same shape as the experimental data up to about 25 degrees. From there to about 55 degrees, the data show a marked divergence. Hauer and Kelly describe a region of flow unsteadiness at 55 degrees which is attributed to a rapid transition between an axial and a transverse flow pattern. Above this region of unsteady flow, the comparison shows another divergence, but at a different degree of error.

Much of the error in the comparison seems to come from the values of the cross-flow drag coefficient used since the computations gave excellent comparisons to 55 degrees and then severe overpredictions to 90 degrees, if a laminar value were used. The difficulty lies in the uncertainty involved in predicting the transition from laminar to turbulent flow, and the rate of recovery of the drag coefficient above the transition point. Reference 11 presents several different cases which could apply, but the selection of the proper one would probably be based on prior knowledge of the experimental data. Transition for a cylinder in cross-flow usually occurs at a diameter-based Reynolds number of 500,000, but this may vary by as much as 200,000. If the test case lies within this region of Reynolds numbers, the actual transition Reynolds number would have to be known to permit selection of the proper cross-flow drag coefficient.

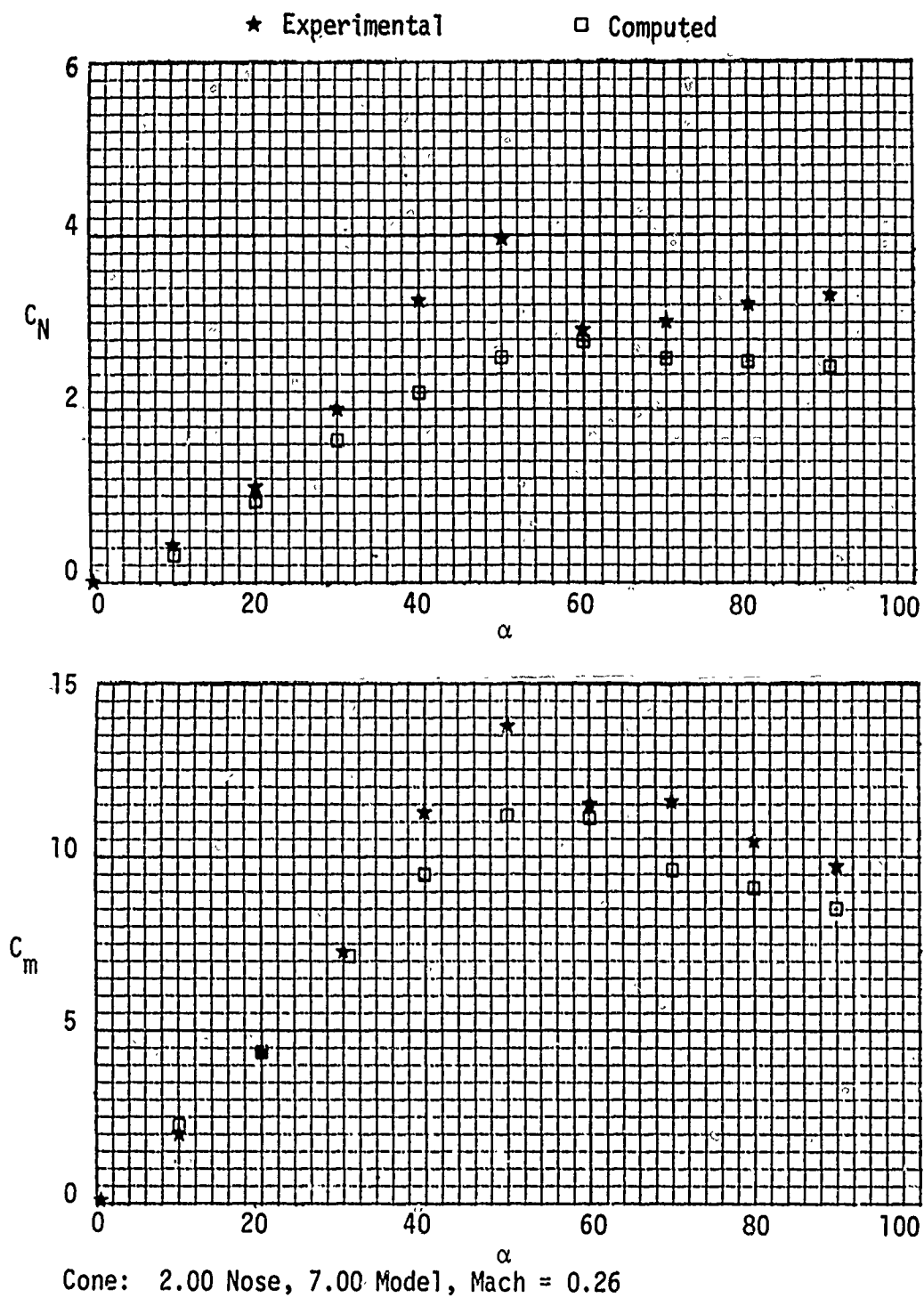
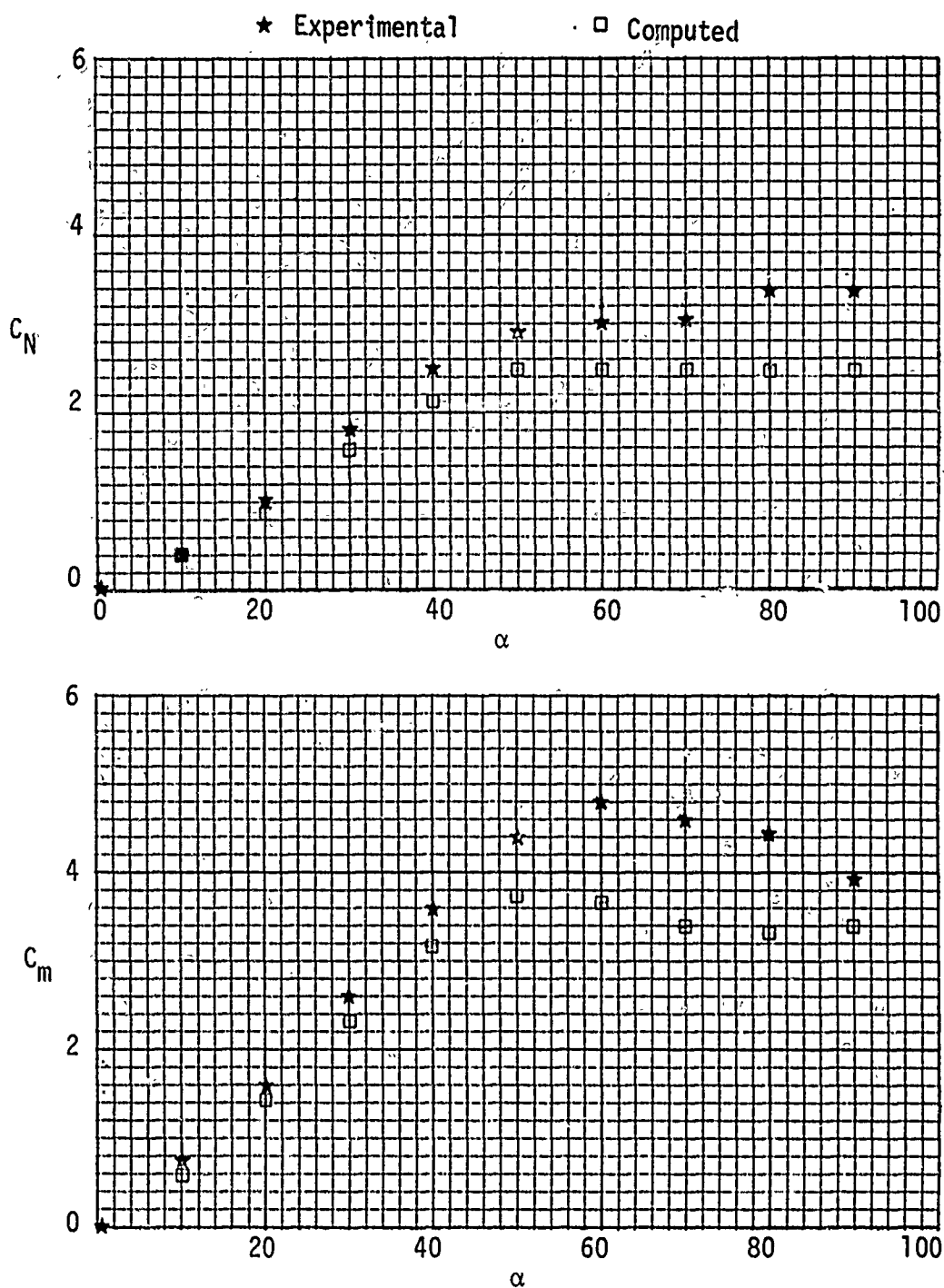


Figure 11. Comparisons to Experimental Data-Subsonic (Reference 15)



Ogive: 4.00 Nose, 7.00 Model, Mach = 0.26

Figure 11. (Concluded)

2. SUPERSONIC

The supersonic runs (Figure 12) were made with an input value for DCNDA. The slope used for input either was taken from the curve in Reference 14, or was computed from the experimental data between zero and five degrees angle of attack. This computation can be used because the various runs show that potential effects account for 95 percent or more of the total normal force coefficient in this region.

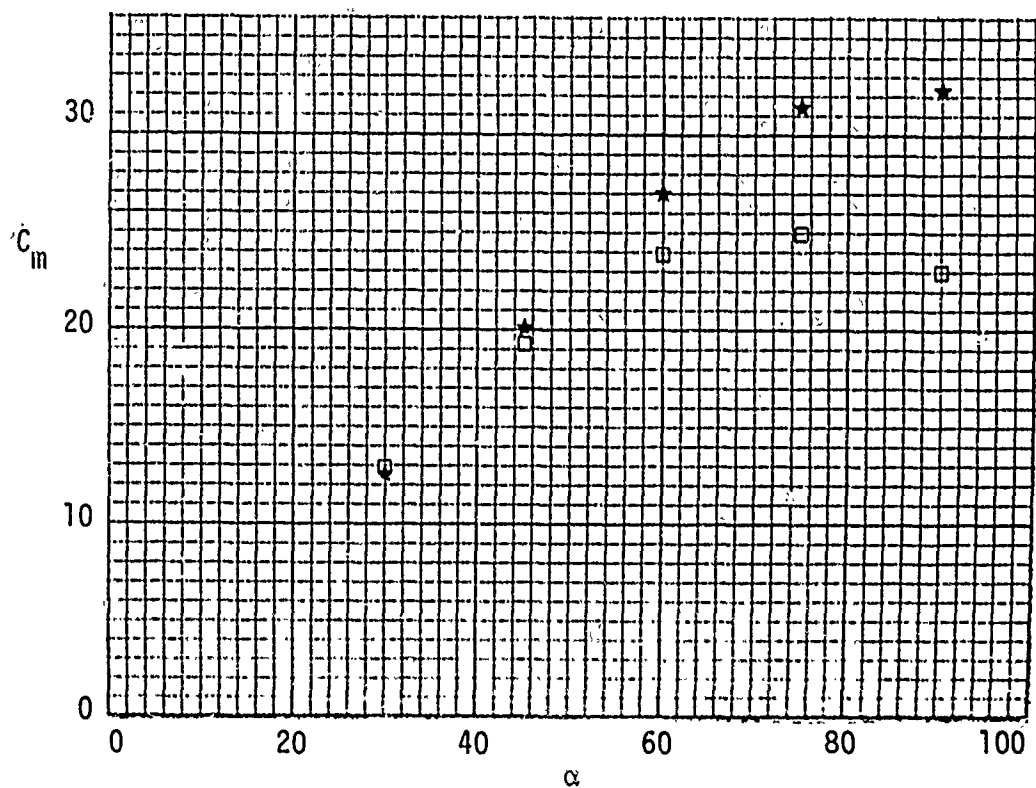
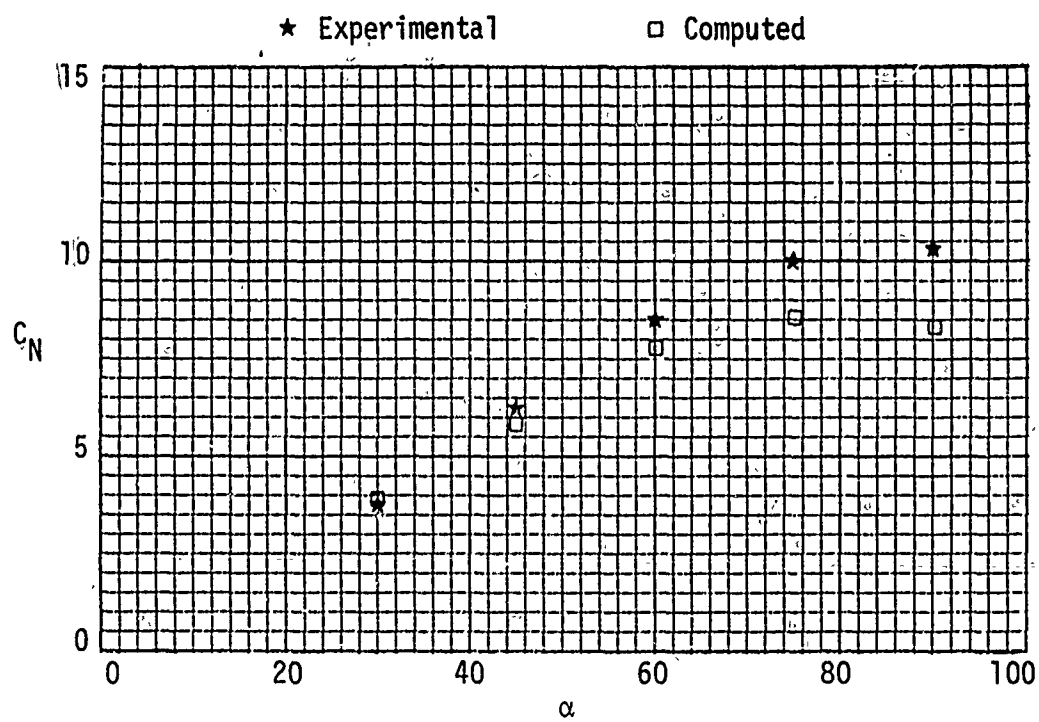
The runs show excellent agreement with the data presented by Penland in Reference 13. The agreement in the hypersonic region is excellent, since the flow approaches the conditions that satisfy the Newtonian theory. The agreement is slightly better than that produced by the Modified Newtonian theory. The data used were in the form of lift and drag coefficients referenced to planform area, but a short program on desk-top computer converted the data to normal force coefficient referenced to base area. The error introduced by these computations is not significant for the purpose of comparison.

The comparisons at Mach 2.37, 2.98, and 3.90 require additional consideration. In an effort to determine n , the 90 degree angle-of-attack runs with cylindrical noses were used to ascertain the effects of Mach number. When the experimental data were converted to useable form, the drag coefficient exceeded the value for an infinite cylinder. Such a condition is contrary to all previous knowledge of this type of flow, and an error is indicated. Since the test runs were made with a wall-mounted sting, the corrections for the mounting condition may contain some error. However, the data are useful for plotting the shape of the curve and were adequate for the original report. The wall mounting limited the data start to 30 degrees and prevented a check on the test apparatus at zero angle of attack. Therefore, the source of the apparent error cannot be evaluated.

3. INDICATED IMPROVEMENTS

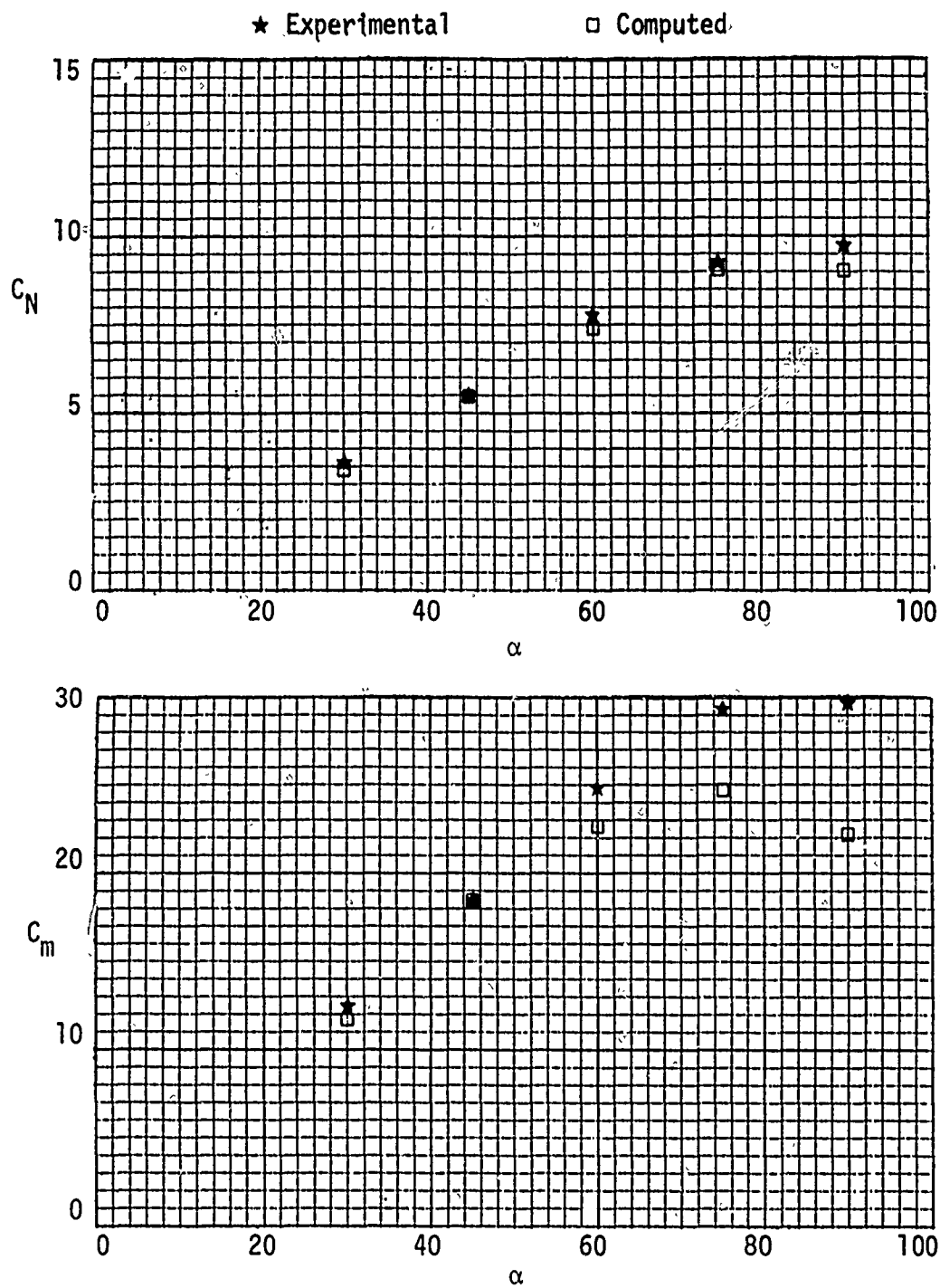
As the program developed, several areas were indicated where an increase in complexity might improve the results; however, the return from the additional effort would be low. Also, the lack of experimental data for correlation with the theoretical results precluded any real value in an attempt to improve the accuracy of the method. If valid data were available and if greater accuracy were required, some improvement in the results would be possible.

The best candidate area for improving accuracy would be the drag coefficient in the region of transition Reynolds numbers. A method of reading into the computer the transition Reynolds number, based on surface roughness and other pertinent factors, could be used to adjust the transition induced dip in the C_{d_c} versus Reynolds number curve. Certainly,



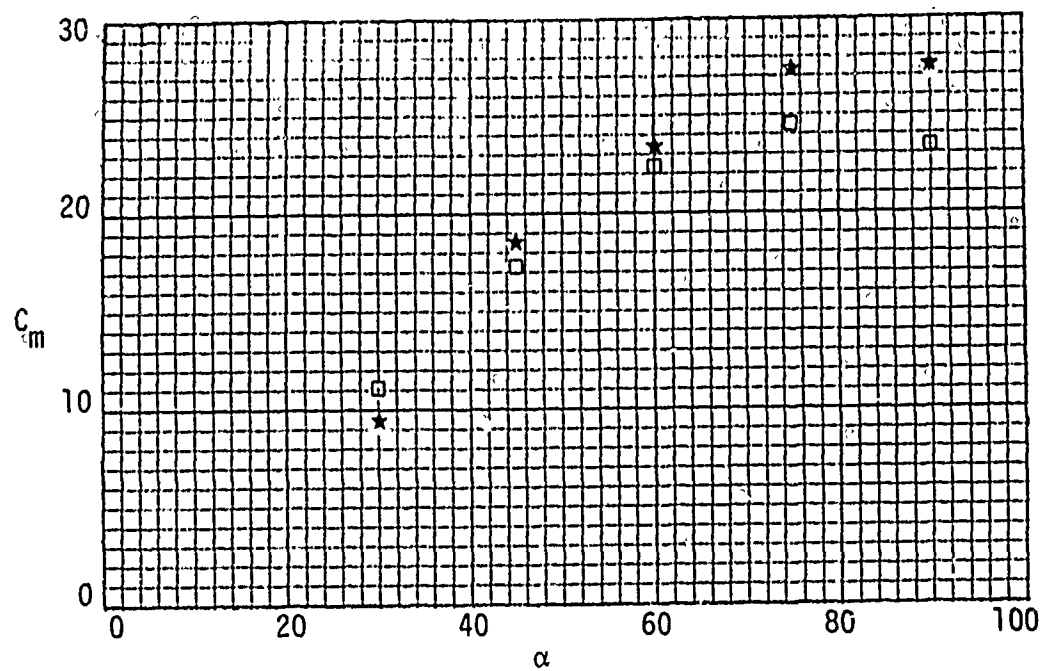
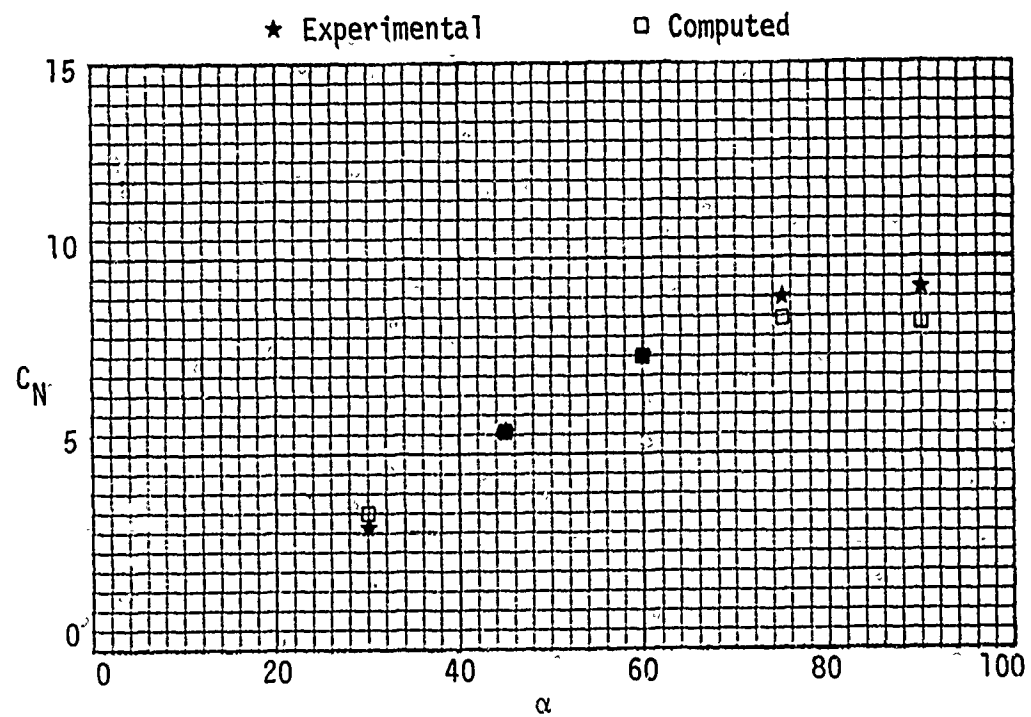
Ogive: 5.00 Nose, 7.00 Model, Mach = 2.37

Figure 12. Comparisons to Experimental Data - Supersonic (Reference 16)



Ogive: 5.00 Nose, 7.00 Model, Mach = 2.98

Figure 12. (Continued)



Ogive: 5.00 Nose, 7.00 Model, Mach = 3.90

Figure 12. (Continued)

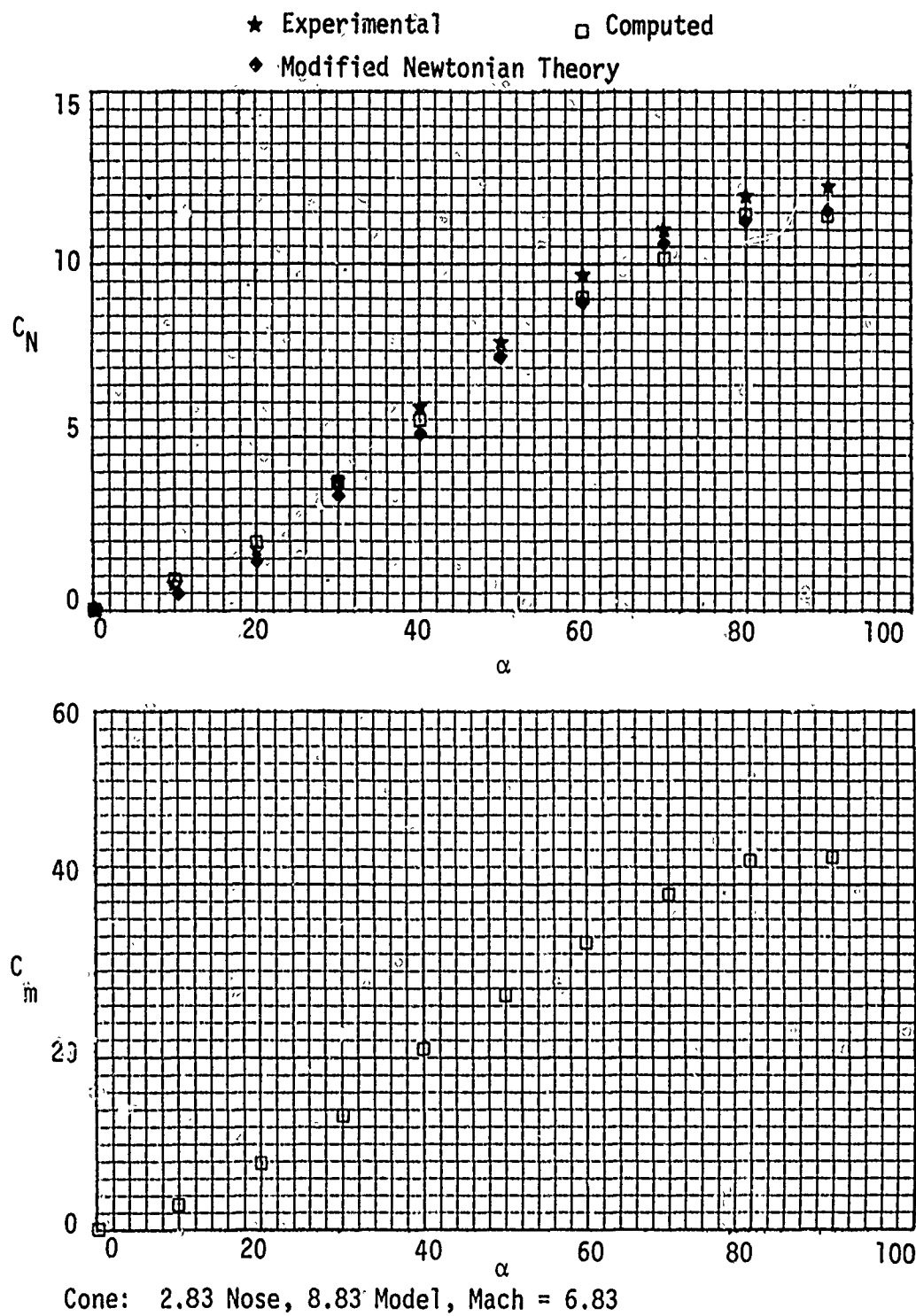
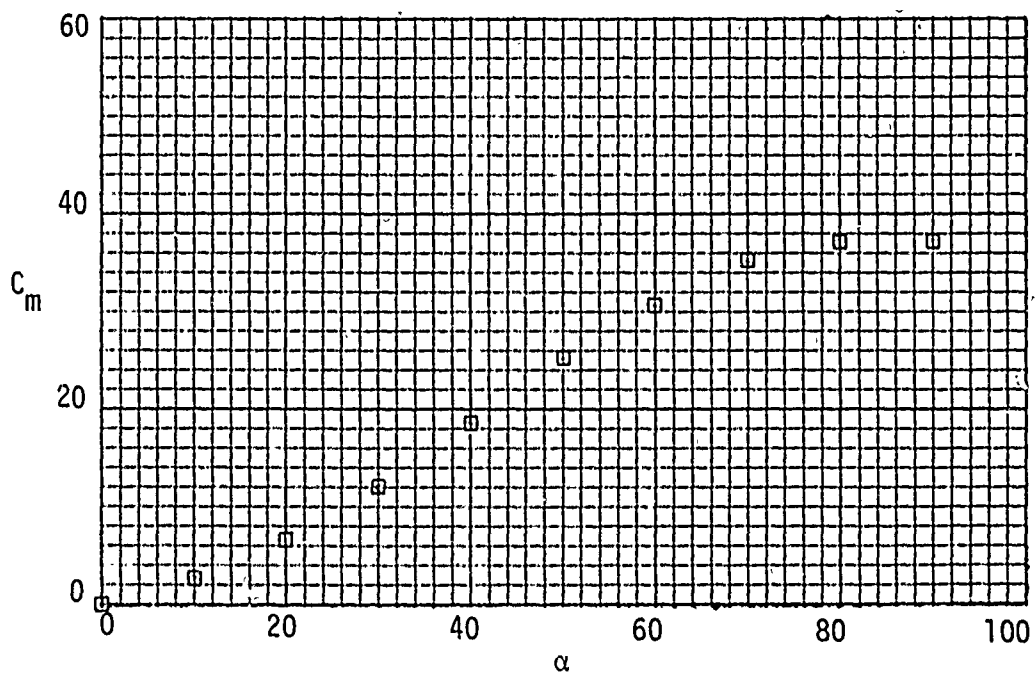
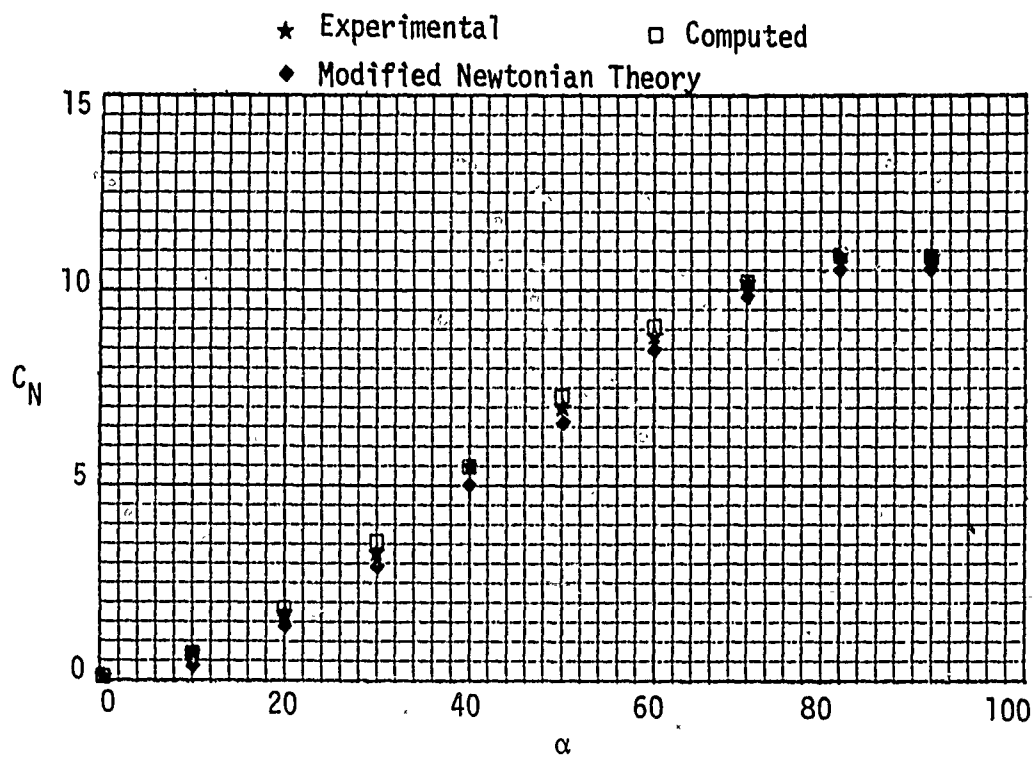


Figure 12. (Continued) (Reference 17)



Cone: 1.87 Nose, 7.87 Model, Mach = 6.83

Figure 12. (Concluded)

additional experimental data in the subsonic range would be required for a significant improvement in this function. More attention to the change from axial to transverse flow dominance could lead to a factor to define its manner and causes. Since both the axial and the transverse flows are involved in transition, and since transition is, at best, not a very predictable phenomenon, a reliable prediction may not be possible.

There are other improvement areas which would give lesser benefits in the improvement of accuracy, and they are mentioned in the order in which they appear in the program.

The volume in the subsonic subroutine assumes an inscribed cone for noses which are not true cones. The radius function could be expanded, or an additional function could be added, to provide a value of volume that would be more accurate for non-conical noses. In particular, this modification would yield better results for the blunter class of power series and parabolic noses.

Since the DCNDA function is approximate, it could easily be improved with additional experimental data. The insertion of experimental data on the input data cards would be the easiest method of correcting this source of error.

The theta subroutine is an averaging process, and it is necessary that theta be averaged for the apparent mass factor. However, when using the nose angle to correct η , the local value of theta would be more accurate for noses which are not true cones.

All the functions that are approximated with line segments could be fitted with higher order curves that would be more accurate.

Any of the factors mentioned might produce some refinement in the accuracy of the predicted aerodynamic characteristics; however, the added complexity is not justified at this time, since experimental data for actual verification are not available. In addition, some of the recommended techniques require experimental data for their implementation. Further, it is a primary goal of this study to retain a minimum of complexity. Additional study should be performed to improve the technique, but without significantly increasing the level of complexity.

SECTION VI

FUTURE DEVELOPMENT

The most significant improvement that might be made to the program would be to include more complex models. The first additions might be nose blunting and boattailing of the afterbody, since each of these could be quite readily incorporated in the present program with only minor modifications. The addition of fins, wings, control surfaces, model irregularities, and changes in shape to include other than bodies of revolution are some of the extensions that would be desirable. These additions require extensive effort for theoretical development, as well as large amount of experimental data; however, the results would be most valuable to future designers and analysts.

The requirements of the Air Force, the intended use of the program, and the success of early advances in complexity would determine how much extension should be undertaken. At this time, the program development confirms the basic theories involved and verifies the value of the computer as a basic research tool in this area.

REFERENCES

1. Munk, Max M., The Aerodynamic Forces on Airship Hulls, NACA Rep No. 184, 1924.
2. Kelly, Howard R., The Estimation of Normal Force and Pitching Moment Coefficients for Blunt-Based Bodies of Revolution at Large Angle of Attack, NOTS TM-998, May 27, 1953
3. Kelly, Howard R., The Estimation of Normal Forces and Pitching Moment Coefficients for Blunt-Based Bodies of Revolution at Large Angles of Attack, Journal of the Aeronautical Sciences, Vol. 1, No. 1, August 1954, pp. 549-555, 565.
4. Allen, H. Julian, and Edward W. Perkins, A Study of Effects of Viscosity on Flow Over Slender Inclined Bodies of Revolution, NACA Rep. No. 1048, 1951.
5. Ward, G. N., Supersonic Flow Past Slender Pointed Bodies, Quarterly Journal of Mechanics and Applied Mathematics, Vol. 2, Part 1, pp. 75-97, March 1949.
6. Goldstein, S., Modern Developments in Fluid Dynamics, Oxford, 1938.
7. Schwabe, M., Pressure Distribution in Nonuniform Two-Dimensional Flow, NACA-TM-1039, 1943.
8. Hill, J. A. F., Forces on Slender Bodies at Angles of Attack, Naval Supersonic Laboratory, Massachusetts Institute of Technology, R-a 100-59, May 9, 1950.
9. Upson, Ralph H., and W. A. Klikoff, Application of Practical Hydrodynamics to Airship Design, NACA Rep. No. 405, 1931.
10. Van Dyke, Milton D., First- and Second-Order Theory of Supersonic Flow Past Bodies of Revolution, Journal of the Aeronautical Sciences, Vol. 18, No. 3, p. 161-178, 216, March 1961.
11. Hoerner, Sigward F., Fluid Dynamic Drag, Published by the author, 1958
12. Gowen, Forrest E. and Edward W. Perkins, Drag of Circular Cylinders for a Wide Range of Reynolds Numbers and Mach Numbers, NACA TN-2960, 1953.
13. Penland, Jim A., Aerodynamic Characteristics of a Circular Cylinder at Mach Number 6.86 and Angles of Attack up to 90°, NACA TN-3861, 1957. (Supersedes NACA RM L54A14.)

REFERENCES

1. Munk, Max M., The Aerodynamic Forces on Airship Hulls, NACA Rep No. 184, 1924.
2. Kelly, Howard R., The Estimation of Normal Force and Pitching Moment Coefficients for Blunt-Based Bodies of Revolution at Large Angle of Attack, NOTS TM-998, May 27, 1953
3. Kelly, Howard R., The Estimation of Normal Forces and Pitching Moment Coefficients for Blunt-Based Bodies of Revolution at Large Angles of Attack, Journal of the Aeronautical Sciences, Vol. 1, No. 1, August 1954, pp. 549-555, 565.
4. Allen, H. Julian, and Edward W. Perkins, A Study of Effects of Viscosity on Flow Over Slender Inclined Bodies of Revolution, NACA Rep. No. 1048, 1951.
5. Ward, G. N., Supersonic Flow Past Slender Pointed Bodies, Quarterly Journal of Mechanics and Applied Mathematics, Vol. 2, Part 1, pp. 75-97, March 1949.
6. Goldstein, S., Modern Developments in Fluid Dynamics, Oxford, 1938.
7. Schwabe, M., Pressure Distribution in Nonuniform Two-Dimensional Flow, NACA-TM-1039, 1943.
8. Hill, J. A. F., Forces on Slender Bodies at Angles of Attack, Naval Supersonic Laboratory, Massachusetts Institute of Technology, R-a 100-59, May 9, 1950.
9. Upson, Ralph H., and W. A. Klikoff, Application of Practical Hydrodynamics to Airship Design, NACA Rep. No. 405, 1931.
10. Van Dyke, Milton D., First- and Second-Order Theory of Supersonic Flow Past Bodies of Revolution, Journal of the Aeronautical Sciences, Vol. 18, No. 3, p. 161-178, 216, March 1961.
11. Hoerner, Sigward F., Fluid Dynamic Drag, Published by the author, 1958
12. Gowen, Forrest E. and Edward W. Perkins, Drag of Circular Cylinders for a Wide Range of Reynolds Numbers and Mach Numbers, NACA TN-2960, 1953.
13. Penland, Jim A., Aerodynamic Characteristics of a Circular Cylinder at Mach Number 6.86 and Angles of Attack up to 90°, NACA TN-3861. 1957. (Supercedes NACA RM L54A14.)

14. Grimminger, G., E. P. Williams, and G. B. W. Young, Lift on Inclined Bodies of Revolution in Hypersonic Flow, Journal of Aeronautical Sciences, Vol. 17, No. 11, pp. 675-690, November 1950.
15. Hauer, Herbert J., and Howard R. Kelly, The Subsonic Aerodynamic Characteristics of Spinning Cone-Cylinders and Ogive-Cylinders at Large Angles of Attack, NAVORD Report 3529, 1955.
16. Smith, Fred M., A Wind Tunnel Investigation of the Aerodynamic Characteristics of Bodies of Revolution at Mach Numbers of 2.37, 2.98 and 3.90 at Angles of Attack to 90°, NASA TM X-311, 1960.
17. Penland, Jim A., Aerodynamic Force Characteristics of a Series of Lifting Cone and Cone-Cylinder Configurations at a Mach Number of 6.83 and Angles of Attack up to 130°, NASA TN D-840, 1961.

APPENDIX

The following block diagrams are intended to show the various relationships of the different parts of the program to each other and to the Main Program. Only those subprograms which utilize another subprogram are included. These diagrams are generalized by the various parts of the subprogram being considered and should not be construed to be flow charts. The equations necessary to write the flow charts have already been presented.

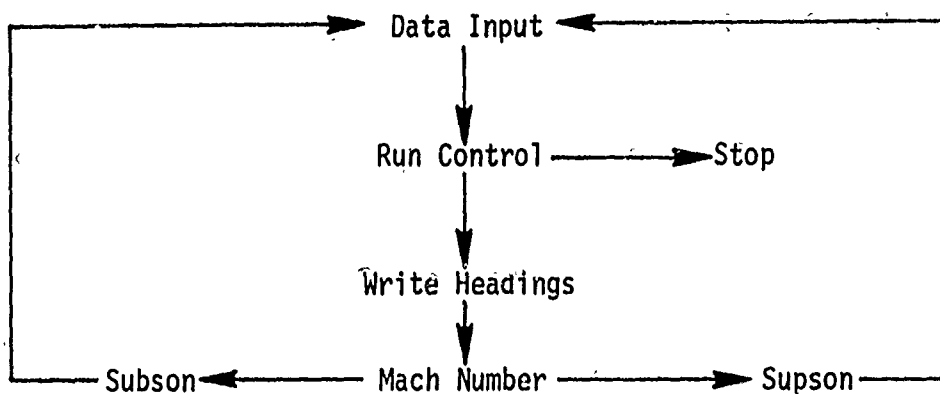
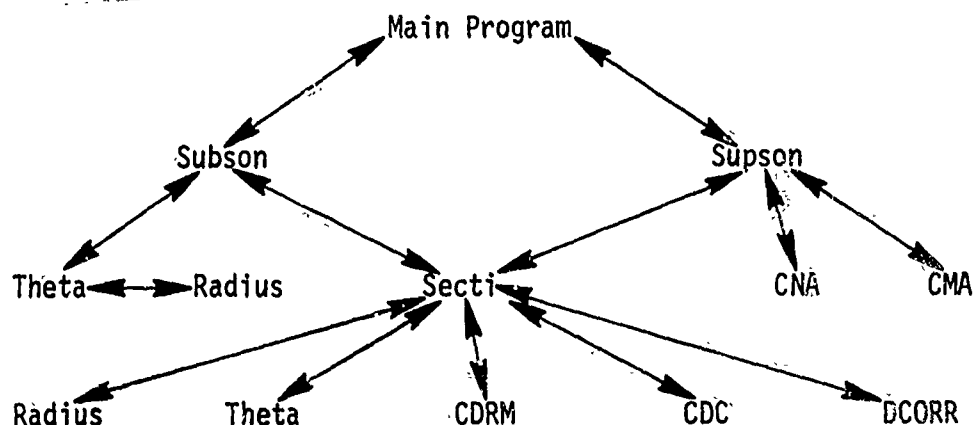


Figure I-1. Main Program

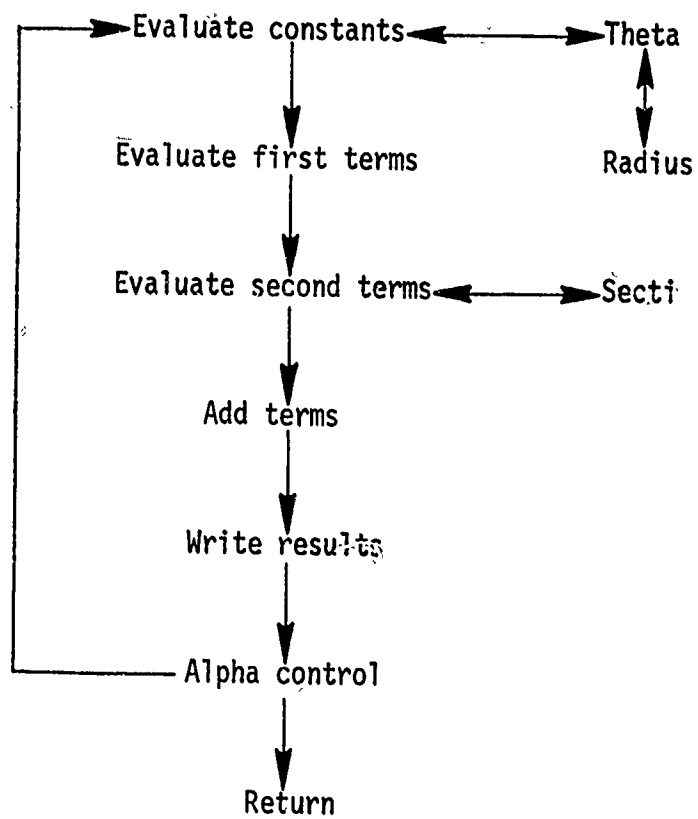


Figure I-2. Subson Subprogram

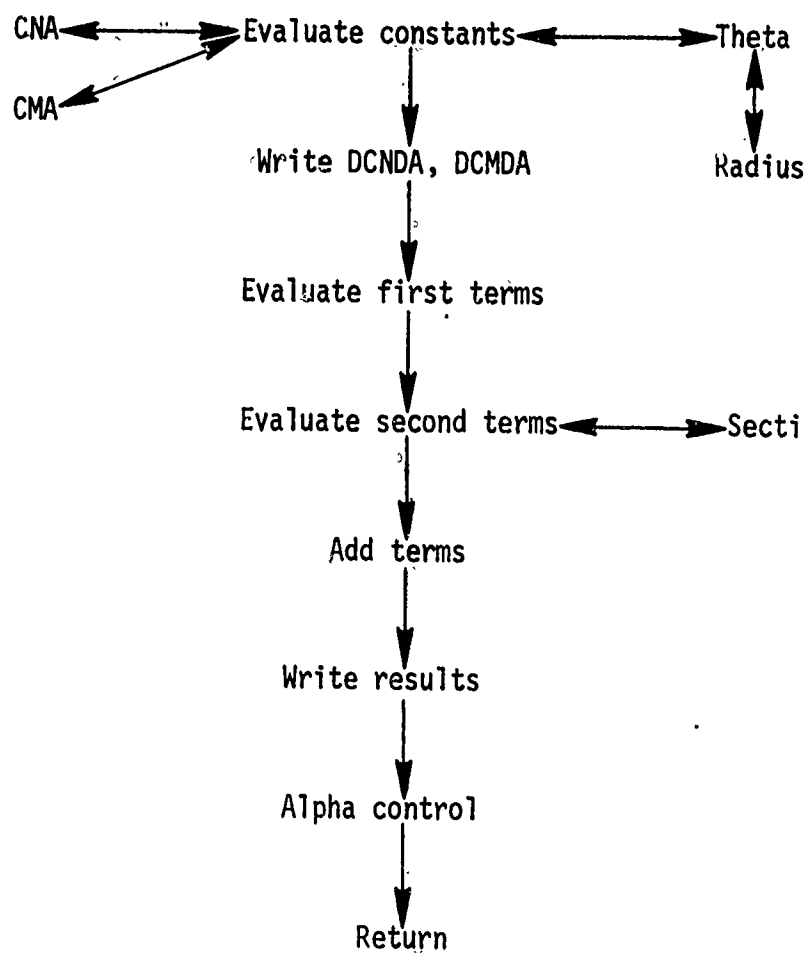


Figure I-3. Supson Subprogram

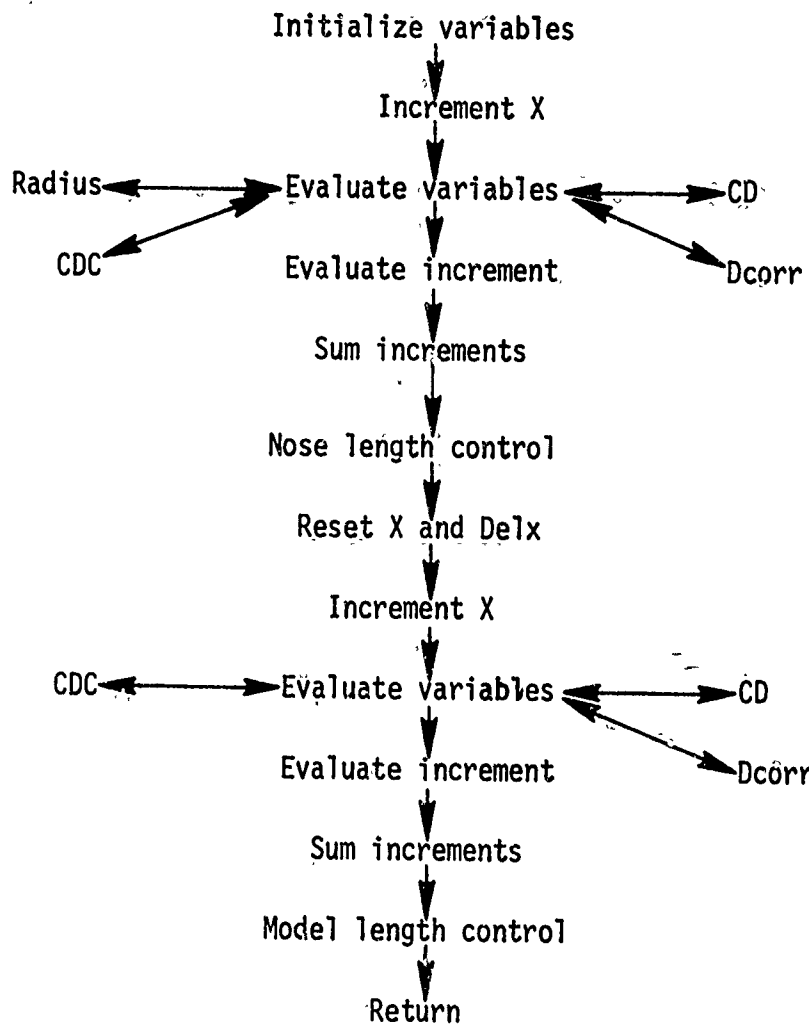


Figure I-4. Secti Subprogram